November 2015

Evaluation of Ferrate Preoxidation for Drinking Water Treatment

Joseph E. Goodwill

Evaluation of Ferrate Preoxidation for Drinking Water Treatment

A Dissertation Presented

by

JOSEPH E. GOODWILL

Submitted to the Graduate School of the

University of Massachusetts Amherst in partial fulfillment

of the requirements for the degree of

DOCTOR OF PHILOSOPHY

September 2015

Department of Civil and Environmental Engineering

Evaluation of Ferrate For Drinking Water Treatment

A Dissertation Presented

by

JOSEPH E. GOODWILL

Approved as to style and content by:

_____

John E. Tobiason, Chair

_____

David A. Reckhow, Member

_____

Jessica D. Schiffman, Member

_____

Richard N. Palmer, Department Head

Civil and Environmental Engineering Department

DEDICATION

To my advisor, Dr. John E. Tobiason, for giving me a chance.

ACKNOWLEDGEMENTS

Funding for this research was provided by the United States Environmental Protection Agency, Grant No. 83560201. I am grateful for the financial support from the Aquarion Water Company, the AWWA Larson Aquatic Research Support Scholarship, the AWWA American Water Scholarship, and the NEWWA George E. Watters Scholarship.

Several other people and organizations have made contributions to this research effort including the Battelle Memorial Institute; Richard Ross of WesTech Inc.; the numerous utilities that provided water, and data; Jacob Hirsh, Ruthanne Paradise, and S. Piril Ertem, all of UMass Amherst, for their assistance conducing various analyses.

I have been fortunate to be part of an outstanding team of researchers with whom I collaborated on this work, including the members of my committee John Tobiason, Dave Reckhow and Jessica Schiffman, as well as fellow students Yanjun Jiang, Joseph Gikonyno, John Martin, Josh Cunningham, Mark Hagemann, and Xuyen Mia.

I gratefully acknowledge the love and support of my parents, Carl and Monica Goodwill, and my wife, Wystan Carswell, my brothers, John and Steve Goodwill, and my friend, Kellen Graham, throughout this process.

ABSTRACT

EVALUATION OF FERRATE PREOXIDATION FOR DRINKING WATER TREATMENT

SEPTEMBER 2015

JOSEPH E. GOODWILL, B.S., LAFAYETTE COLLEGE

M.S., UNIVERSITY OF MASSACHUSETTS AMHERST

Ph.D., UNIVERSITY OF MASSACHUSETTS AMHERST

Directed by: Dr. John E. Tobiason

Ferrate (Fe(IV)) has been proposed as a viable alternative for pre-oxidation in drinking water treatment (Jiang & Lloyd, 2002; Sharma, Kazama, Jiangyong, & Ray, 2005). The primary advantages of ferrate include a strong oxidation potential without the formation of halogenated by-products. In addition, the by-product of ferrate oxidation, ferric iron (Fe(III)), may have beneficial impacts on downstream particle destabilization and removal processes. Also, ferrate has disinfectant properties and may also provide pathogen inactivation in drinking water (Sharma et al., 2005). However, despite these advantages, there is a dearth of research experience that examines the implications of using ferrate for treating actual drinking water sources for potable water production.

Studies were conducted evaluating the nature of particles that result from ferrate reduction in a laboratory water matrix and in a natural surface water with a moderate amount of dissolved organic carbon. Particle characterization included size, surface charge, morphology, X-ray photoelectron spectroscopy and transmission Fourier transform infrared spectroscopy. Characteristics of ferrate resultant particles were compared to particles formed from dosing ferric chloride, a common water treatment coagulant. In natural water, ferrate addition produced significantly more nanoparticles than ferric addition. These particles had a negative surface charge, resulting in a stable colloidal suspension. In natural and laboratory matrix waters, the ferrate resultant particles had a similar charge versus pH relationship as particles resulting from ferric addition. Particles resulting from ferrate had morphology that differed from particles resulting from ferric iron, with ferrate resultant particles appearing smoother and more granular. X-ray photoelectron spectroscopy results show ferrate resultant particles contained Fe_2O_3, while ferric resultant particles did not. Results also indicate potential differences in the mechanisms leading to particle formation between ferrate reduction and ferric hydrolysis.

An analysis of soluble manganese oxidation by ferrate (Fe(VI)) was executed at the bench-scale, in a laboratory water matrix, both with and without the presence of natural organic matter (NOM). In the laboratory water matrix without NOM, the oxidation of Mn(II) by Fe(VI) was found to follow a stoichiometry of 2 moles Fe(VI) to 3 moles Mn(II), resulting in reduced, particulate Fe(III) and oxidized, particulate Mn(IV). The size distribution of resulting particles included significant amounts of nanoparticles. The

observed stoichiometric ratio held for multiple initial Mn(II) concentrations and pH values. The presence of NOM did not significantly affect the stoichiometry, indicating limited competitive oxidant demand. Fe(VI) dosages above the stoichiometric ratio produced Mn(VII). The rate of the Mn(II) oxidation reaction was fast relative to typical time scales in drinking water treatment, with an estimated second order rate constant of approximately 1.0×10^{4} M^{-1} s^{-1} at pH 9.2.

A laboratory assessment of ferrate for drinking water treatment was conducted, including batch and continuous flow experiments on several different natural water samples. In batch experiments, ferrate preoxidation enhanced the removal of ultraviolet light absorbing compounds (UV254) by subsequent coagulation in a minority of water samples, while the majority of samples showed no improvement. In continuous flow experiments, ferrate was incorporated into small-scale models of existing treatment plants. In general, ferrate preoxidation improved finished water turbidity, UV254 absorbance and disinfection by-product formation as compared to no preoxidation and preoxidation with Mn(VII). However, for one natural water, improvements were similar in magnitude to those achieved by adding the same mass of Fe(III) in place of Fe(VI) prior to a formal coagulation step. Particulate iron resulting from Fe(VI) reduction was effectively destabilized and removed via coagulation and filtration. Ferrate may be a viable technology for drinking water treatment systems; and present a better alternative to existing oxidants by providing disinfection and oxidation of inorganics without negative impacts to downstream stream processes. The benefits of adding ferrate are likely to vary based on raw water quality and treatment goals

TABLE OF CONTENTS

Page

ACKNOWLEDGEMENTS v

ABSTRACT vi

LIST OF TABLES xiii

LIST OF FIGURES xiii

CHAPTER

1. OVERVIEW AND INTRODUCTION 1

2. CHARACTERIZATION OF PARTICLES RESULTING FROM FERRATE PREOXIDATION 6

2.1 Introduction 6

2.2 Materials and Experimental Methods 8

2.2.1 Particle Formation Reaction 9

2.3 Analytical Methods 10

2.3.1 Ferrate and Iron Concentrations 10

2.3.2 Particle Size 10

2.3.3 Zeta Potential 12

2.3.4 Streaming Current Measurements and Charge Titrations 12

2.3.5 Organic Carbon 12

2.3.6 Scanning Electron Microscopy 13

2.3.7 X-ray Photoelectron Spectroscopy 13

2.3.8 Fourier Transform Infrared Spectroscopy. 13

2.3.9 Reagents 14

2.4 Results 14
2.4.1 Particle Size 14
2.4.2 Surface Charge 19
2.4.3 Fractionation of NOM 22
2.4.4 Morphology 23
2.4.5 Surface Analysis 24
2.5 Discussion 26
2.5.1 Potential Differences in Precipitation Mechanism 26
2.5.2 Role of DOC, and Differences in Particle Characteristics 28
2.5.3 Implications for Water Treatment 30
3. OXIDATION OF MANGANESE(II) WITH FERRATE: STOICHIOMETRY, KINETICS, PARTICLES, AND IMPACT OF ORGANIC CARBON 33
3.1 Introduction 33
3.2 Materials and Methods 35
3.2.1 Water Quality 35
3.2.2 Oxidation Reaction 35
3.2.3 Kinetic Studies 36
3.3 Analytical Methods 37
3.3.1 Iron and Manganese Concentrations 37
3.3.2 Particle Size 38
3.3.3 Natural Organic Matter 38
3.3.4 X-ray Photoelectron Spectroscopy 39
3.3.5 Reagents 40
3.4 Results 40
3.4.1 Stoichiometry 40
3.4.2 Reaction Kinetics 43

3.4.3 Characterization of Resulting Particles 45
3.4.4 Impact of NOM 49
3.5 Discussion 51
3.5.1 Reaction Stoichiometry and Kinetics 51
3.5.2 Particle Characteristics 54
3.5.3 Impact of NOM 54
3.5.4 Implications for Drinking Water Treatment 55
4. LABORATORY ASSESSMENT OF FERRATE FOR DRINKING WATER TREATMENT 57
4.1 Introduction 57
4.2 Materials and Methods 60
4.2.1 Batch Experiments 60
4.2.2 Continuous Flow Experiments 62
4.2.3 Analytical Methods—Batch Experiments 64
4.2.4 Analytical Methods—Continuous Flow Experiments 64
4.2.5 Analytical Methods—Organic Carbon and DBPs 65
4.2.6 Source Waters 65
4.3 Results 67
4.3.1 Batch experiments 67
4.3.2 Continuous flow experiments 69
4.4 Discussion 78
4.4.1 Ferrate and coagulation—batch experiments 78
4.4.2 Ferrate and filtered water quality—continuous flow experiments 79
4.4.3 Engineering and operational considerations 81
5. CONCLUSIONS 83

APPENDIX: SUPPORTING INFORMATION 86

BIBLIOGRAPHY 92

LIST OF TABLES

Table Page

Table 4.1. Water quality information for all batch experiment water; OFD = optimal ferric chloride dose, SUVA = specific ultra-violet absorbance 66

Table 4.2. Full scale and continuous flow experimental parameters..... 67

Table 4.3. Optimal ferric dose with and without ferrate preoxidation; coagulation pH = 5.5 68

Table A.1 Water quality characteristics of Atkins Water..... 86

Table A.2 Regression results from linear relationship between Fe(VI) dose and Mn(II) oxidized; DI water matrix: 1 mM HCO_3^-, $Mn(II)_i$ = 4.9 μM and 9.8 μM; NOM water matrix: 1 mM HCO_3^-, $Mn(II)_i$ = 4.9 μM and 9.8 μM, TOC = 1.75 mg/L; (yo = y-intercept, SE = standard error, a = slope) 88

LIST OF FIGURES

Figure Page

Figure 1.1. Schematic of simplified water treatment processes including ferrate preoxidation 4

Figure 1.2 Schematic of common possible pathways for ferrate reaction as a preoxidant in drinking water treatment 5

Figure 2.1 Number concentration (#/mL) of ferrate and ferric resultant particles in laboratory and natural water matrices; 1mM HCO_3^-, pH = 6.2, Fe = 3 mg/L. Each bar represents the mean of 10 measurements, counted in predefined size channels with error bars representing the positive and negative of one standard deviation 15

Figure 2.2 Particle size distribution for ferrate and ferric resultant particles in natural water matrix; 1mM HCO_3^-, pH = 6.2, Fe = 3 mg/L. Each bar represents the mean of 12 measurements, counted in predefined size channels with error bars representing the positive and negative of one standard deviation 17

Figure 2.3 Size of iron particles using filter fractionation; lab and natural water matrix: 1mM HCO_3^-, pH = 6.2, Fe = 3 mg/L; phosphate water matrix: 10 mM PO_4^{-3}, pH = 6.2, Fe = 3 mg/L (LP: large particles, SP: small particles) 18

Figure 2.4 Streaming current results of charge titration of ferrate and ferric resultant particles in laboratory and natural water matrix; 1 mM HCO_3^-, Fe = 3 mg/L 21

Figure 2.5 NOM of natural water matrix following ferrate and ferric iron addition and filtration; 1 mM HCO_3^-, pH = 6.2, Fe = 3 mg/L (NPOC: Non-purgeable organic carbon) 23

Figure 2.6 Micrograph of particles from ferric (A) and ferrate (B) addition in natural water 24

Figure 2.7 Photoelectron spectra in the Fe $2p^{3/2}$ and O 1s regions of ferric and ferrate resultant particles from a DI water matrix (1 mM HCO_3^-, pH = 6.2) and a Fe_2O_3 (hematite) standard 25

Figure 3.1 Linear relationship between Fe(VI) dose and Mn(II) oxidized in a laboratory water matrix; 1 mM HCO_3^-, pH = 7.5 and 6.2, $Mn(II)_i$ = 4.9 μM and 9.8 μM; N = 48 41

Figure 3.2 Relative absorbance of a super stoichiometric ferrate dose sample (e.g., in situ), and a MnO_4^- solution. In situ sample: DI water matrix; pH = 6.2; HCO_3^- = 1mM; $Mn(II)_i$ = 5.5 μM; Fe(VI) dose = 11 μM. $NaMnO_4$ sample: pH = 6.2; HCO_3^- = 1 mM 42

Figure 3.3 Mn(VII) formed during oxidation of Mn(II) with super stoichiometric dosages of Fe(VI). $Mn(II)_i$ = 4.9 μM; HCO_3^- = 1 mM 43

Figure 3.4 Apparent Fe(VI) concentrations during oxidation of dissolved Mn(II); BO_3^{-3} = 0.2 mM, pH as indicated, Fe(VI) initial = 75 μM, Mn(II) initial = 113 μM 44

Figure 3.5 Mn 3p (7P) photoline spectrum for Mn oxide standards and particles resulting from Mn(II) oxidation by Fe(VI). For oxidation reaction, pH = 7.5, HCO_3^- = 1 mM 46

Figure 3.6 Size fractionation of iron and manganese particles resulting from oxidation of Mn(II) with Fe(VI), on a mass of metal basis. In samples with NOM, TOC = 1.75 mg/L, DOC = 1.5 mg/L. HCO_3^- = 1 mM; $Mn(II)_i$ = 4.9 μM; Fe(VI) = 3.3 μM (LP = Large Particles, SP = Small Particles, NP = Nanoparticles). 48

Figure 3.7 Linear relationship between Fe(VI) dose and Mn(II) oxidized in deionized water matrix with natural organic matter; TOC = 1.75 mg/L; 1 mM HCO_3^-, pH = 7.5 and 6.2, $Mn(II)_i$ = 4.9 μM and 9.8 μM; N = 19 49

Figure 4.1. Batch experimental method diagram; UV254=absorbance of ultra-violet light at 254 nm, GF/F=glass fiber fine, TOC=total dissolved carbon, DOC=dissolved organic carbon, DBPFP=disinfection byproduct formation potential 61

Figure 4.2. UV254 absorbance following coagulation at optimum $FeCl_3$ dose with and without ferrate preoxidation; coagulation pH = 5.5, borate buffer = 1 mM 68

Figure 4.3. UV254 absorbance, turbidity and headloss results from continuous flow experiments 71

Figure 4.4. Counts of particles between 2 μm and 100 μm in diameter from light-blockage instrument in filter effluent with and without ferrate preoxidation 72

Figure 4.5. Profile of iron concentrations and fractions across continuous flow experiment processes for South Deerfield water with ferrate preoxidation; CT = contact tank, Mix = following addition of coagulant, pH control and rapid mixing, AC = adsorption clarifier, Eff = filter effluent; Fe(VI) dose = 50 μm 73

Figure 4.6. Continuous flow and full scale disinfection byproduct formation potential results for Atkins and South Deerfield water; For Atkins, Fe(VI)= 25 μM, For South Deerfield, Fe(VI)=50 μM 75

Figure 4.7. UV254 absorbance and turbidity results for continuous flow experiments on South Deerfield water utilizing no preoxidation (Polymer Only), Fe(III) and Polymer, Fe(VI) and Polymer, and Mn(VII) and Polymer; Fe(III) = 3 mg/L as Fe, Fe(VI) = 50 μM (2.9 mg/L as Fe), Mn(VII) = 10 μM 76

Figure 4.8. Disinfection byproduct formation potential results for continuous flow experiments on South Deerfield water; Polymer= 6 mg/L as product, Fe(VI) = 50 μM (2.9 mg/L as Fe), Mn(VII)=10 μM, Fe(III) = 3 mg/L as Fe 77

Figure A.1 Boxplot of zeta potential of ferrate and ferric resultant particles in lab and natural water matrices; 1 mM HCO_3^-, pH = 6.2, Fe = 3 mg/L 86

Figure A.2 Transmission FTIR spectra of ferric and ferrate resultant particles 87

Figure A.3 Micrograph of particles from ferric (A) and ferrate (B) addition in natural water 87

Figure A.4 Streaming current results from coagulant charge analyzer; 1 mM HCO_3^-, Mn(II) initial = 11 μM, Fe(VI) dose = 7.5 μM 88

Figure A.5 Normalized Fe(VI) concentration decay measured via absorbance at 510nm with second order rate constant numerical approximation model; pH = 9.2; BO_3^{-3} = 0.2 mM, Fe(VI) initial = 75 μM, Mn(II) initial = 113 μM; estimated $k_2 = 1.0\times10^4$ M^{-1} s^{-1} 89

Figure A.6 Photoelectron spectra in the Fe $2p^{3/2}$ region of particles resulting from ferrate decay (e.g., Fe(VI) only), oxidation of Mn(II) by Fe(VI), and an Fe_2O_3 standard (hematite) 90

Figure A.7 TOC and DOC Mn(II) water matrix following various ferrate dosages; 1 mM HCO_3^-, (NPOC, nonpurgable organic carbon). Each bar represents the mean of 3 measurements, with error bars representing the positive and negative of one standard deviation 91

CHAPTER 1

OVERVIEW AND INTRODUCTION

Water is perhaps the most essential environmental resource as it is not only required for life, but also vital to economic and social prosperity. However, a global water crisis is emerging driven by increasing demands from water resources strained by exploitation, pollution, and climate change. Concurrently, a period of global economic stagnation is limiting the resources available to increase water treatment. These combined factors place significant stress on water systems.

Given this combination of drivers, technological innovation is needed to strengthen water systems, creating more capacity, energy efficiency, and adaptability. These improvements entail producing larger amounts of higher quality water from possibly degrading supplies while decreasing energy usage.

Ferrate (Fe(IV)) has been proposed as an emerging "green chemical" for drinking water treatment. Ferrate has a high oxidation potential, and the by-product of ferrate oxidation, ferric iron (Fe(III)), may have beneficial impacts on downstream particle destabilization and removal processes. Also, ferrate has disinfectant properties and may also provide pathogen inactivation in drinking water (Sharma, 2007).

The fundamental advantage of ferrate is that the by-products of oxidation with ferrate are beneficial inputs for subsequent water treatment processes. As a strong oxidant, ferrate can supplant ozone or chlorine-based oxidants. The resulting iron material can then undergo adsorption and precipitation reactions (e.g., coagulation) and lead to removal of contaminants such arsenic and organic matter through particle removal processes, thus decreasing the need for an additional coagulant. Ferrate is also a powerful disinfectant, and can inactivate pathogens. Thus ferrate may be considered as a potential alternative to chlorine or ultra-violet light. These multiple modes of action with ferrate provide potential efficiency that water treatment utilities find valuable. This characteristic of ferrate also makes it an attractive option to smaller utilities with limited resources, which may especially struggle to adapt to increasing water system stress. Ferrate can increase environmental equality by enabling fair distribution of environmental benefits, as there are few impediments to its use such as significant economic investment or changes to existing mechanical systems.

However, despite these advantages, there is a dearth of research experience that examines the implications of using ferrate to produce drinking water. The oxidation of various specific compounds with ferrate has been examined, but most of these studies have been conducted in a laboratory setting using phosphate buffers and incorporating other simplifying conditions that are rarely applicable to drinking water treatment practice. Likewise, the potential for beneficial use of the ferric iron (Fe(III)) by-product has been proposed, but not researched conclusively. Furthermore, the disinfection properties of

ferrate have been documented, but it is currently not possible to earn log inactivation credits from a regulatory standpoint.

Therefore, the overall objective of this research is to evaluate the impacts of using ferrate in drinking water treatment systems. To accomplish this, ferrate was incorporated into bench-scale and pilot-scale treatment systems, mimicking the full-scale treatment processes of numerous participating utilities. Experiments with these systems focused on the effect of ferrate treatment on parameters of importance in water treatment such as disinfection by-product formation potential (DBPFP), turbidity, metals concentrations, and total organic carbon (TOC) concentration.

In the work presented in this dissertation, ferrate has been exclusively considered as a potential preoxidant, with addition occurring before the primary particle destabilization and physical separation processes. This was primarily motivated by the assumption that ferric iron particles resulting from ferrate reduction would require removal by downstream treatment processes. A general DWT schematic is shown in Figure 1.1, including ferrate preoxidation.

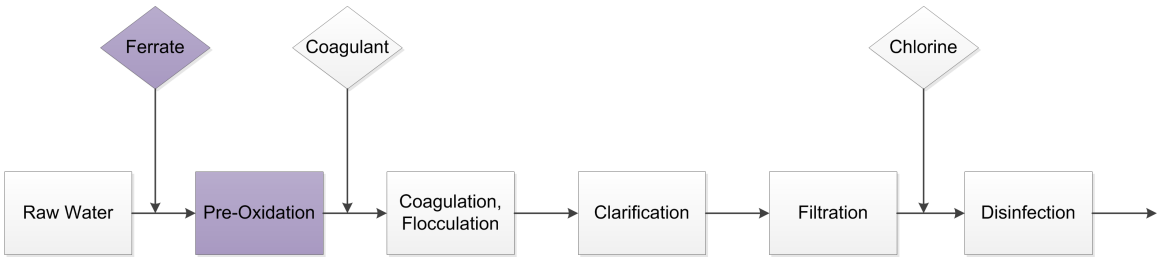

Figure 1.1. Schematic of simplified water treatment processes including ferrate preoxidation

A summary of common possible ferrate reaction pathways is shown in Figure 1.2. The possible impacts of adding ferrate to a raw water are multiple and complex. Very few studies have focused on the impacts of adding ferrate for drinking water treatment in a manner that accounts for multiple possible outcomes

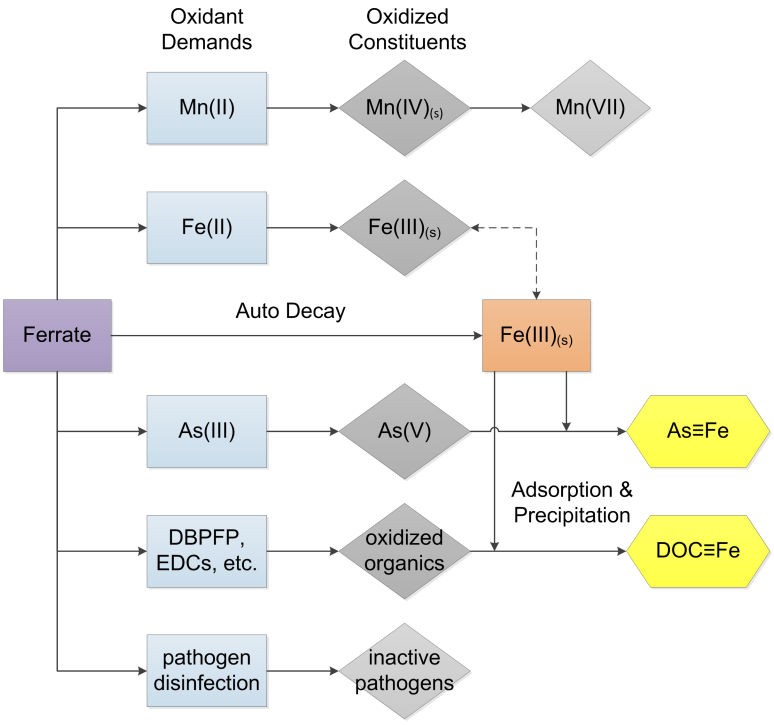

Figure 1.2 Schematic of common possible pathways for ferrate reaction as a preoxidant in drinking water treatment

The scope of this dissertation focused on three of the potential pathways shown in Figure 1.2) the characterization of ferrate resultant particles, 2) the oxidation of manganese(II) by ferrate, and 3) a laboratory investigation of ferrate oxidation of natural organic matter such as DBPFP and the subsequent impact on adsorption and the formation and subsequent removal of particulate Fe and organic matter.

CHAPTER 2

CHARACTERIZATION OF PARTICLES RESULTING FROM FERRATE PREOXIDATION

Modified from originally published version (Goodwill, J.E., Jiang, Y., Reckhow, D.A., Gikonyo, J., Tobiason, J.E., 2015. Characterization of Particles from Ferrate Preoxidation. Environ. Sci. Technol. 49, 4955–4962. doi:10.1021/acs.est.5b00225)

2.1 Introduction

Pre-oxidation, the addition of an oxidant to raw water as a first treatment step, is practiced by some drinking water utilities to achieve various water treatment goals. Commonly used pre-oxidants include permanganate, chlorine dioxide and ozone. While often effective at achieving treatment goals, some of these oxidants also have disadvantages, primary among them is the production of regulated byproducts(Gordon et al., 1990; von Gunten, 2003; Werdehoff and Singer, 1987) and relative operational complexity.

Ferrate (Fe(VI)) has been proposed as an alternative for pre-oxidation in drinking water treatment.(Jiang and Lloyd, 2002; V. Sharma, 2002) The primary potential advantages of ferrate include a strong oxidation potential and disinfection properties (Sharma, 2007) without the formation of hazardous by-products (DeLuca et al., 1983). In addition, the by-product of ferrate reduction, ferric iron (Fe(III)), may have beneficial impacts on downstream water treatment processes and has been proposed as a coagulant.(Sharma et al., 2005) The potential applicability of ferrate to both pre-oxidation as well as

coagulation processes may lend an inherent operational simplicity when compared to other pre-oxidant options. Despite these potential advantages, there is a dearth of research that examines the use of ferrate in treating natural drinking water sources.

Specifically, there has been little direct examination of the characteristics of particulate Fe(III) resulting from ferrate reduction and the direct comparison of this material to the particulate Fe(III) resulting from the addition of a ferric coagulant. Yet, the assumption persists that these two sources of iron yield particulate matter that has similar characteristics in natural water. While there have been numerous studies on the use of ferrate to oxidize specific contaminants (Sharma, 2011), a large portion of the studies use a 1-10 mM phosphate buffer. Phosphate complexes iron(III), decreasing the formation of precipitates (Huang et al., 2001) which can complicate experiments. Ferrate behavior in phosphate buffers can be used to predict oxidation effects in natural waters without added phosphate (Lee et al., 2005a, 2005b), and research on these more homogenous systems is necessary; however, the use of phosphate obscures the impact of ferrate resultant particles in the context of natural water pre-oxidation. For example, ferrate was shown to decay more rapidly in the presence of particles resulting from ferric chloride addition, as compared to being in the presence of particles resulting from ferrate reduction (Jiang et al., 2015). This difference in ferrate reactivity suggests significant differences in these two particle types that could have important implications in water treatment.

The objectives of this study were to: (1) examine and compare the characteristics of the solids resulting from ferrate reduction and ferric hydrolysis in a laboratory matrix water and a natural drinking water source; (2) examine the potential for differences in precipitation mechanism between these two particle types and (3) consider how these characteristic and mechanistic differences may impact the use of ferrate pre-oxidation for drinking water treatment.

2.2 Materials and Experimental Methods

Water Quality. Three types of water were used in this study: a deionized (DI) laboratory grade water with a carbonate buffer, DI water with a phosphate buffer, and raw water from the Atkins Reservoir (Amherst, MA, USA). Atkins Reservoir water quality is summarized in Appendix A (Table A.1). In the laboratory grade water with carbonate buffer and the natural Atkins Reservoir water case, a 1mM carbonate buffer was added and pH was controlled to 6.2. This was required in the natural water case due to low alkalinity. The carbonate buffer was chosen over other buffer options (e.g., phosphate or borate) to replicate natural water conditions. In the phosphate water matrix, 10 mM of phosphate was added as sodium phosphate and pH similarly controlled to 6.2. A 10 mM concentration of phosphate was chosen to replicate other work examining oxidation of organic contaminants with ferrate (Sharma and Mishra, 2006; Yang et al., 2011). All experiments were conducted at 21 degrees Celsius.

2.2.1 Particle Formation Reaction

Particles were formed by adding 3 mg/L as Fe of ferrate or 3 mg/L as Fe of ferric chloride to water samples. The iron was added to 750 mL of sample in a batch reactor, during 60 seconds of rapid mixing (G ~ 250 sec^{-1}). Mixing intensity was then reduced (G ~ 60 sec^{-1}) to simulate flocculation or oxidation contact time in drinking water treatment. pH was monitored and adjusted to remain at 6.2 using drop-wise addition of 1M NaOH or 1M HCl as required.

Ferrate was added by first making a concentrated (500 mg/L as K_2FeO_4 or 2.53 mM FeO_4^{-2}) stock solution by dissolving potassium ferrate in DI water. A volume of this stock solution was then immediately added to the reactor as required to yield the desired dosed concentration. Ferric was added by first making a concentrated (1 g/L as Fe, or 17.9 mM Fe) stock solution by dissolving ferric chloride salt in DI water. These solutions were added immediately after production to the rapidly mixed reactor to eliminate concentration gradients.

3 mg/L as Fe was chosen as a realistic dose of ferrate based on other batch and continuous flow drinking water treatment experiments (Goodwill et al., 2014; Y. Jiang et al., 2014). Ferrate dosages of this magnitude effectively oxidized phenolic endocrine disrupters (Lee et al., 2005b) and arsenic(III) (Lee et al., 2003) in natural waters. A pH of 6.2 was selected to fall within a common pH range for iron-based coagulation and

flocculation in water treatment as well as the pH resulting from pre-oxidation with ferrate in some natural waters (Goodwill et al., 2014).

2.3 Analytical Methods

2.3.1 Ferrate and Iron Concentrations

Ferrate concentrations were measured using an ABTS indicator method (Lee et al., 2005a). Iron concentrations were measured using a colorimetric method (APHA et al., 2005) adapted for use with a colorimeter (DR2400, Hach) with duplicate-samples analyzed by inductively coupled plasma mass spectrometry (ICP-MS). Results for the two iron measurement techniques were generally within 5% agreement.

2.3.2 Particle Size

Particle size was measured using a light blockage instrument (2400 PS, Chemtrac) and a dynamic light scattering (DLS) instrument (Zetasizer Nano ZS, Malvern Instruments). Both instruments were checked for calibration using secondary standards of known particle sizes.

In the case of the light blockage instrument, 50 mL of solution was drawn through the instrument using the built-in peristaltic pump at a flow rate of 100 mL/min, following 30 seconds (50 mL) of purging. Each analysis included 10 measurements in each pre-

defined size range channel. The range of measurable sizes was between 2 μm and 100 μm; particles outside of this range (e.g., nanoparticles) are not measured with this instrument.

The Malvern Zetasizer measurement method included 12 replicates. The angle of detection was set at 173 degrees of backscatter. Particles measured by the DLS instrument above 1 μm in size were disregarded due to low intensities, and very low signal-to-noise ratios. All results reported are the intensity weighted average (Z-average) size.

Particle size was also characterized by fractionation with several filters of progressively smaller effective size exclusions (Carlson et al., 1997). Filters used in the fractionation process included a fine glass fiber (GF/F) filter with an effective size exclusion cut-off of 0.7 µm (GE Whatman), a microfiltration membrane filter (MF) with a pore-size of 0.2 µm (Nuclepore Polycarbonate, Track-Etch Membrane, GE Whatman) and a 30 kDa regenerated cellulose membrane ultra-filter (UF) (EMD Millipore). Solids retained on the GF/F filter were operationally defined as large particles (LP). Solids passing the GF/F filter but retained on the 0.2 µm filter were defined as small particles (SP). Solids passing the 0.2 µm filter, but retained on the 30 kDa UF were defined as colloidal (e.g., nanoparticles), and material passing the 30 kDa UF was considered dissolved. New filters were used in each separation to minimize the formation of a particle cake. Results are reported on a mass of iron basis.

2.3.3 Zeta Potential

Electrophoretic mobility was also measured using the Malvern Zetasizer Nano ZS, and converted to zeta potential using the Smoluchowski equation.

2.3.4 Streaming Current Measurements and Charge Titrations

Streaming current measurements were made using a coagulant charge analyzer (CCA) (Chemtrac CCA 3000). In-situ measurements were taken after the 30 minutes of reaction time, while stirring continued. Readings of this initial condition were taken, and then 1M HCl was added to the solution in a drop-wise manner while the pH and corresponding streaming current were monitored.

2.3.5 Organic Carbon

Organic carbon (OC) was analyzed by measuring non-purgeable organic carbon (NPOC) using a Shimadzu TOC-VCPH carbon analyzer. The instrument was calibrated with dilutions of a 10 mg/L (as carbon) potassium hydrogen phthalate standard. The samples were acidified with 6N HCl solution and purged with nitrogen to remove inorganic carbon prior to analysis. Samples were analyzed in triplicate with the mean value reported. OC measurements conformed to Standard Methods Section 5310B (APHA et al., 2005).

2.3.6 Scanning Electron Microscopy

Samples were prepared for scanning electron microscopy (SEM) by drying 50 mL of solution at 104 C. The resulting solids were removed, and mounted onto aluminum tabs with carbon tape. The samples were coated with an Edwards Xenosput XE200 xenon-magnetron sputter. Approximately 5 nm of platinum was deposited on the samples. SEM micrographs were taken using a Zeiss EVO 50 SEM, operating at an accelerating voltage of 15 keV, and a working distance ranging from 4 mm to 6 mm. Numerous images of each sample were taken and visually assessed for significant differences in morphology.

2.3.7 X-ray Photoelectron Spectroscopy

Samples of resultant particles from the laboratory matrix were prepared for x-ray photoelectron spectroscopy (XPS) in the same manner as SEM samples. Analysis was conducted using a Phi Quantum 2000 spectrometer with a monochromatic Al Kα X-ray source operating at 1486.6 eV, 37.5 W. The diameter of the analysis area was approximately 200 μM. The step size was 0.2 eV, and the pass energy was 46.95 eV. XPS was also performed on an Fe_2O_3 standard (hematite, Iron(III) oxide, ≥ 99% purity, Sigma Aldrich). The depth of analysis was estimated to be 3 to 5 nm.

2.3.8 Fourier Transform Infrared Spectroscopy.

Samples of resultant particles from the laboratory matrix were prepared for transmission Fourier transform infrared spectroscopy (FTIR) by a similar drying procedure used for SEM preparation. The resulting solids were mixed with ultra-pure potassium bromide, and pressed into discs. Analysis was executed using a Perkin Elmer Spectra 100 instrument, and included 16 replicate scans.

2.3.9 Reagents

All chemical reagents used were laboratory grade. The ferrate source was potassium ferrate (K_2FeO_4) with 92% purity from Sigma Aldrich (St. Louis, MO). The ferric chloride source was ferric chloride hexahydrate from Fisher Scientific (Waltham, MA). Hydrochloric acid (HCl), sodium hydroxide (NaOH) and sodium phosphate dibasic anhydrous (Na2HPO4) were also purchased from Fisher Scientific. The HCl and NaOH were obtained as a 12 N and 50% solution, respectively.

2.4 Results

2.4.1 Particle Size

The number concentrations of particles measured using the light blockage particle counter for the ferrate and ferric iron addition for the laboratory (no phosphate) and natural water matrices are shown in Figure 2.1

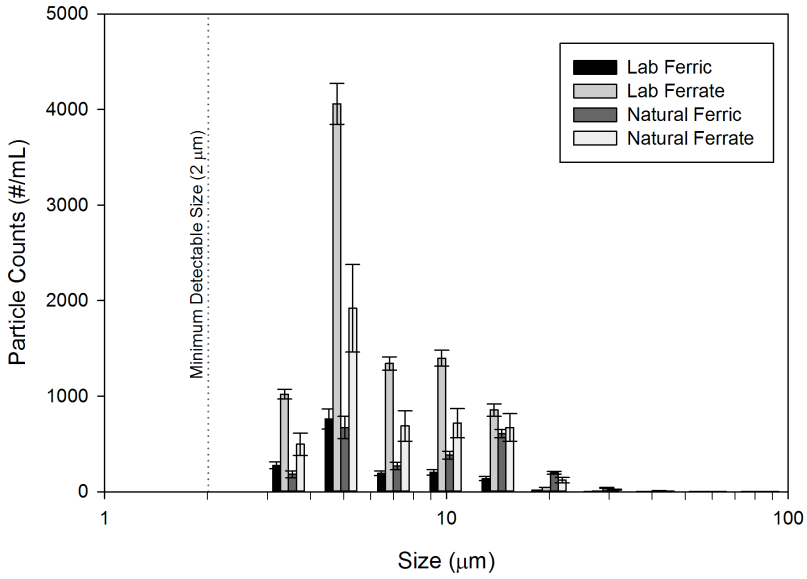

Figure 2.1 Number concentration (#/mL) of ferrate and ferric resultant particles in laboratory and natural water matrices; 1mM HCO_3^-, pH = 6.2, Fe = 3 mg/L. Each bar represents the mean of 10 measurements, counted in predefined size channels with error bars representing the positive and negative of one standard deviation

Results in Figure 2.1 indicate that the majority of particles counted had a diameter between 3 and 20 μm. Particles with a diameter > 100 μm were not present in any case. However, larger flocs were observed in the case of ferric addition to the laboratory water matrix, and also in the natural water matrix, to a lesser extent. These large flocs were likely larger than the reported upper size limit of the instrument. The calculated average particle sizes for counted ferric particles in the laboratory and natural water matrix were 5.8 μm and 8.6 μm, respectively. The calculated average particle sizes for ferrate in the laboratory and natural water matrix were 6.2 and 6.8 μm, respectively. Results in Figure 2.1 indicate that ferrate reduction formed greater numbers of counted particles in both studied water matrices as compared to ferric addition. Also, ferrate reduction formed

fewer total particles in the natural water matrix than in the laboratory matrix, most significantly in the size range ≤ 10 μm. In the laboratory water matrix without phosphate, the total particle number concentration for the ferric and ferrate resultant particles were 1586 #/mL and 8724 #/mL, respectively. In the natural water matrix, the total particle number concentrations for the ferric and ferrate resultant particles were 2366 #/mL and 4641 #/mL, respectively.

Figure 2.2 shows data collected from the DLS instrument for a size range from 10 to 1000 nm, for ferric and ferrate iron addition in the natural water matrix only. Results from the laboratory water matrix are not shown, because instrument intensities were very low, suggesting a lack of an appreciable presence of particles. Results indicate a significant difference between the size distributions for the two iron sources. In the case of ferrate iron addition, the distribution was bimodal, with a significantly lower intensity, secondary peak occurring between 250 nm and 1000 nm.

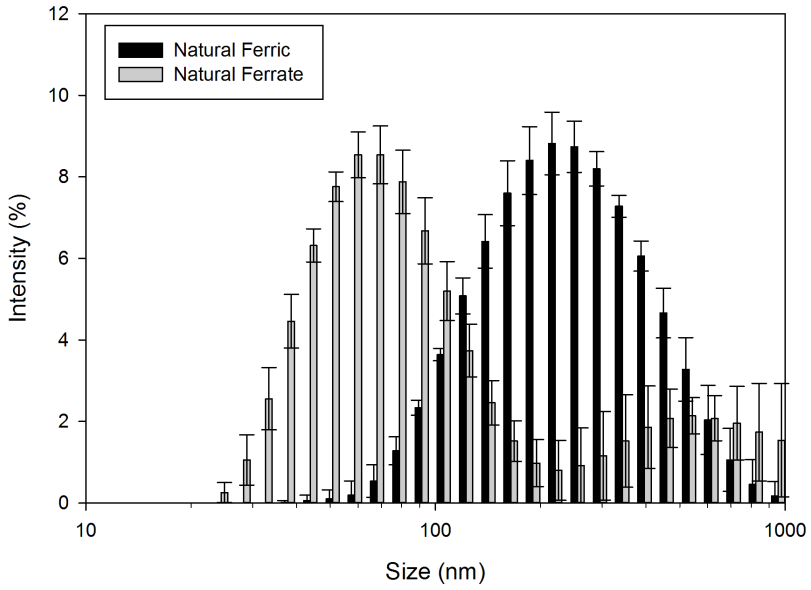

Figure 2.2 Particle size distribution for ferrate and ferric resultant particles in natural water matrix from dynamic light scattering instrument; 1mM HCO_3^-, pH = 6.2, Fe = 3 mg/L. Each bar represents the mean of 12 measurements, counted in predefined size channels with error bars representing the positive and negative of one standard deviation

The Z-average size of particles resulting from ferrate was 172 nm, including all measured intensities. If the secondary peak is excluded, the particle size was 76 nm. Both of these Z-average sizes for ferrate resultant particles are smaller than the 276 nm Z-average size for the ferric iron addition case. Ferrate iron addition produced a significant amount of nanoparticles with diameters less than 100 nm, while the ferric iron addition produced a significant amount of larger particles with diameters greater than 200 nm.

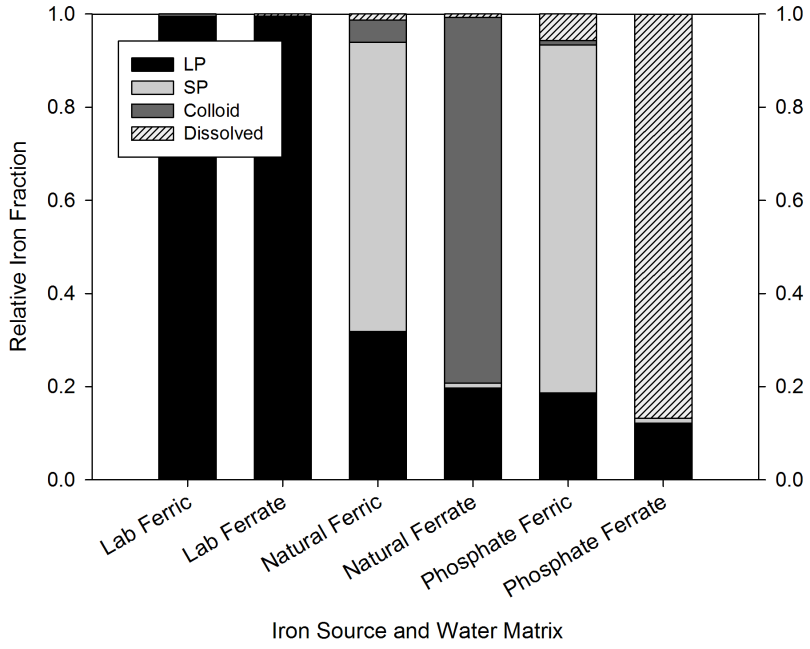

Figure 2.3 Size of iron particles using filter fractionation; lab and natural water matrix: 1mM HCO_3^-, pH = 6.2, Fe = 3 mg/L; phosphate water matrix: 10 mM PO_4^{-3}, pH = 6.2, Fe = 3 mg/L (LP: large particles, SP: small particles)

Figure 2.3 results show clear differences between ferrate produced particles and ferric produced particles in the natural water matrix. In the ferric addition case, 94% of particles were either defined as LP or SP, with 5% defined as colloidal. In the ferrate addition case, 19% was defined as LP, < 1% was defined as SP and 79% was defined as colloidal. In general, these results are supported by DLS instrument output, which showed ferrate addition resulting in a different particle size distribution with more nanoparticles when compared to ferric addition to natural water.

In general, the bimodal distribution of particles measured on the DLS resulting from ferrate reduction in natural water is corroborated by the fractionation results based on iron concentration. Results in Figure 2.3 show that on a mass of iron basis the largest fractions of particles had sizes greater than 700 nm or less than 200 nm, with very little material existing in the 200 to 700 nm size range.

Figure 2.3 fractionation results following addition of ferric and ferrate iron to a 10 mM phosphate buffered laboratory water show significant differences between the two sources of iron. For the ferric iron in phosphate buffer case, approximately 19% of particles were LP, 75% were SP, and 5% were dissolved. These results are similar to the results obtained for ferric iron in the natural water matrix. For the ferrate iron case, approximately 12% of iron was LP, and 87% was dissolved in the phosphate buffer, significantly different than for the natural water where the majority of ferrate resultant iron was in the form of nanoparticles, with a diameter < 200 nm. In the phosphate water matrix, the majority of iron from ferrate remained dissolved, as operationally defined. The results for both ferrate and ferric iron in the phosphate buffer differ greatly from the laboratory water with no phosphate where only large particles were formed.

2.4.2 Surface Charge

Particle surface charge results are included in Appendix A (Figure A.1). Particles resulting from ferric and ferrate addition to the laboratory water (no phosphate) had median zeta potentials of -4.9 mV and -4.8 mV, respectively. A simple t-test of the two

sample populations showed no statistically significant difference; however, there was a significant difference between iron particles in the laboratory and natural waters. In the natural water, the ferric and ferrate resultant particles had median zeta potentials of -24.9 mV and -23.7 mV, respectively. A simple t-test between the two populations showed no statistically significant difference between particles formed from the two iron sources in natural water.

The less negative zeta potentials for both particle types in the laboratory matrix are consistent with the much larger particles in the laboratory waters. Less negative zeta potentials likely indicate less stable particles, which are likely to aggregate. More negative zeta potentials, as observed in the natural water for both particle sources, indicate a more stable colloidal suspension, where aggregation would be limited (Sharp et al., 2006).

The difference in surface charge between laboratory and natural water matrices was also clear in the streaming current results. Figure 2.4 includes the results of a charge titration from an initial pH of 6.2 to a final pH of approximately 3.0. At the initial pH, iron particles in the natural water matrix had significantly more negative surface charge than in the laboratory matrix. Differences in surface charge between the iron types in the same water matrix were relatively small, similar to the zeta potential results.

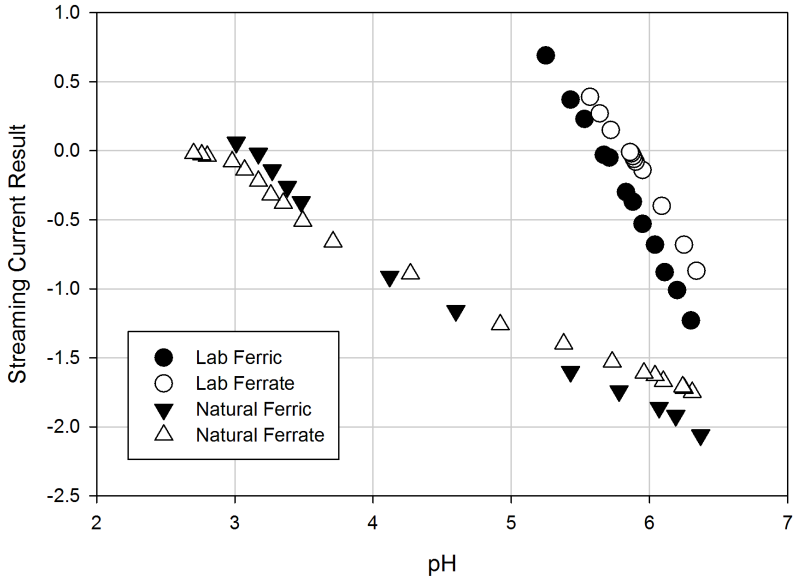

Figure 2.4 Streaming current results of charge titration of ferrate and ferric resultant particles in laboratory and natural water matrix; 1 mM HCO_3^-, Fe = 3 mg/L

Results in Figure 2.4 show differences in charge titration between particles in the two studied water matrices, including pH values at the point of zero charge (PZC). The surfaces of the ferric and ferrate resultant particles show generally similar behavior across the titration pH values in both water matrices. The PZC in the laboratory water matrix for the ferric and ferrate resulting particles occurred at a pH of 5.67 and 5.86, respectively. In contrast, the PZC of ferric and ferrate resultant particles in natural water occurred at pH values of 3.17 and 2.71, respectively.

Zeta potential was also measured on the DLS instrument after reaching the PZC for both particle types, and water matrices, and found to be generally 0 ± 1 mV. The PZC of the

ferric resultant particles in natural water was in agreement with other studies examining similar iron doses and water matrices (Black et al., 1963).

2.4.3 Fractionation of NOM

Figure 2.5 shows NPOC levels for the natural water before and after fractionation. The unfiltered NPOC levels for both ferric and ferrate dosed waters were very similar to levels for the raw water without any iron addition, indicating no destruction of NOM. There was little change in the NPOC concentration following GF filtration for both particle types. Following MF filtration, the NPOC was lower in the sample with ferric iron addition as compared to ferrate addition. This difference is attributed to the association of NOM with the iron particles, and the subsequent separation of these particles and associated NOM from solution. The difference in MF filtrate NPOC between the two particle sources is caused by the majority of ferrate resultant particles passing through the 0.2 μm filter, while the majority of ferric resultant particles are retained (see Figure 2.3). NPOC decreased approximately 25% for both iron cases between no filtration and the UF filtration steps. No attempt was made to adjust the iron dose to optimize for coagulation and removal NOM.

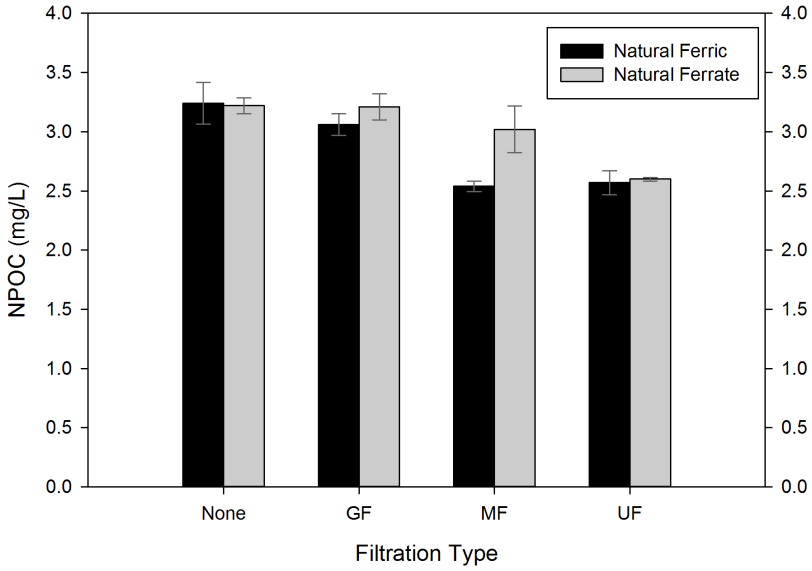

Figure 2.5 NOM of natural water matrix following ferrate and ferric iron addition and filtration; 1 mM HCO_3^-, pH = 6.2, Fe = 3 mg/L (NPOC: Non-purgeable organic carbon)

2.4.4 Morphology

The morphology of ferric and ferrate resulting particles in natural water was examined through the use of SEM. Figure 2.6 shows micrographs of both iron sources taken at approximately 10,000 times magnification. The ferric resultant particles (image A) were roughly textured with angular protrusions. In comparison, the morphology of the ferrate resultant particles was different even though the samples were prepared in the same way. The ferrate resulting particles (image B) were less angular, more rounded and more granular compared to the ferric particles.

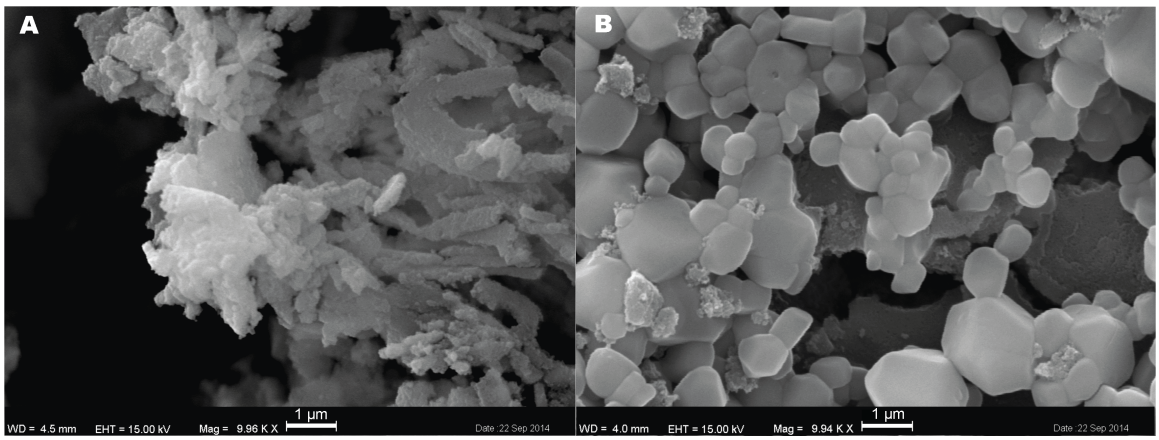

Figure 2.6 Micrograph of particles from ferric (A) and ferrate (B) addition in natural water

SEM micrographs are inherently difficult to interpret when examining heterodisperse, multimodal distributions of particles in a natural water matrix. However, the results do present a significant difference between some of the particles produced by the two different forms of iron addition. More micrographs are including in Appendix A (Figure A.3). The limited amount of nanoparticles shown in each micrograph can be attributed to the agglomerative effect of drying (He et al., 1996).

2.4.5 Surface Analysis

XPS and transmission FTIR were used to determine the characteristics of the iron and oxygen found in the resultant particles. Figure 2.7 includes XPS results for the ferric and ferrate resultant particles, and a Fe_2O_3 (hematite) standard; FTIR spectra are located in Appendix A (Figure A.2).

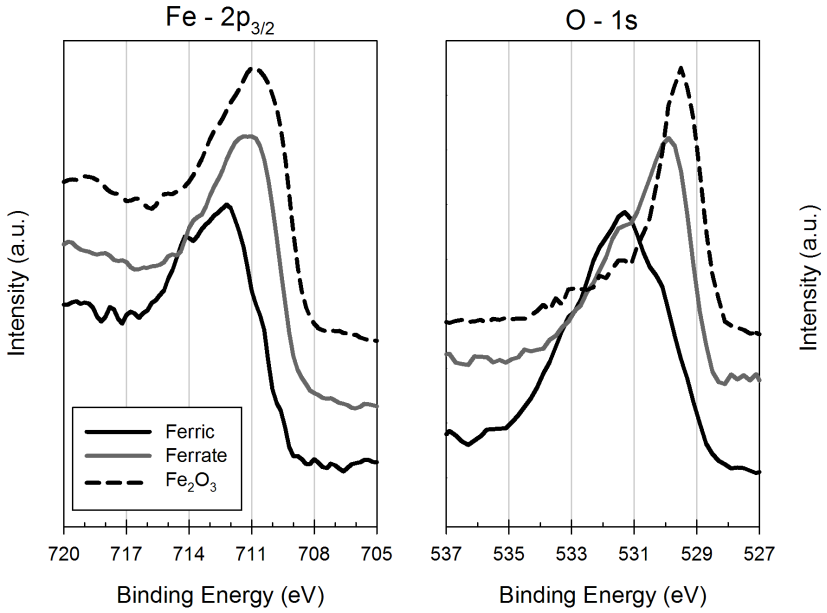

Figure 2.7 Photoelectron spectra in the Fe $2p^{3/2}$ and O 1s regions of ferric and ferrate resultant particles from a DI water matrix (1 mM HCO_3^-, pH = 6.2) and a Fe_2O_3 (hematite) standard

In the Fe $2p^{3/2}$ region, the ferric and ferrate resultant particles had binding energy peaks of 712.1 eV and 711.3 eV, respectively. In the case of ferrate, the peak location is in agreement with previous XPS analysis of ferrate resultant particles (Prucek et al., 2013). The ferric resultant particle peak area was near the binding energy range associated with FeOOH (Moulder et al., 1992). The results indicate different peak locations for the ferric and ferrate resultant particles with the ferrate resultant particles having a spectrum more similar to the Fe_2O_3 standard than the ferric resultant particles.

The spectra in the O 1s region also showed differences between the two particle types with ferric and ferrate resultant particles binding energy peaks of 531.3 eV and 529.9 eV, respectively. The ferrate peak location falls within the binding energy range associated

with Fe_2O_3 (Moulder et al., 1992), and much closer than the ferric particles to the binding energy peak of the Fe_2O_3 standard. The ferric resultant particle O 1s peak also falls in the range associated with hydroxides, and the ferrate resultant particles also had a smaller secondary peak in this range, indicating the presence of some Fe-OH bonds (Moulder et al., 1992).

Results from FTIR (Figure A.2) for both particle types generally showed small, broad peaks, indicating poor crystallinity (Music et al., 1998) and making interpretation difficult. FTIR spectra of ferrate resultant particles had slightly stronger, more defined peaks including peaks at 583 cm^{-1} and 456 cm^{-1}, consistent with Fe_2O_3 (Music et al., 1998; Schwertmann and Cornell, 2008). Strong, discrete peaks in the 800-900 cm^{-1} range that would be consistent with goethite were not observed. Both spectra included peaks between 1500 cm^{-1} and 1300 cm^{-1}, indicating adsorbed carbonate(Schwertmann and Cornell, 2008), and broad peaks at 3400-3450 cm^{-1}, attributable to stretching modes of OH groups or H_2O molecules (Gotić and Musić, 2007).

2.5 Discussion

2.5.1 Potential Differences in Precipitation Mechanism

Differences in characteristics between ferric and ferrate resultant particles suggest differences in precipitation mechanisms. Results from XPS analysis indicate that ferrate reduction yields particles comprised of Fe_2O_3, which was not detected in the ferric resultant particles. This implies that ferrate reduction produces Fe(III) that does not hydrolyze extensively but forms through direct crystallization of Fe_2O_3. This crystalline

form is more stable, and can occur directly from low molecular weight precursors; however, this mechanism is rarely favored kinetically (Duan and Gregory, 2003; Flynn Jr., 1984). Typically, crystallization of $Fe(OH)_3$ occurs through a slower aging processes. This aging process is dependent on several factors, and can be accelerated by the presence of OH^- (Cornell et al., 1989). Conditions within the Fe(VI)-water matrix in this study could produce localized presence of higher OH^- due to the protonation of ferrate at the pH of 6.2, and the OH^- produced by Fe(VI) oxidation of water (V. Sharma, 2002). This could make it appear that Fe_2O_3 precipitated directly relative to the particle formation reaction time. Therefore, it is not possible to determine the exact nature of potential precipitation mechanism differences. The possibility of accelerated aging of ferrate resultant particles would be supported by the similarities in the impact of aged ferric chloride resultant solids and ferrate resultant solids on subsequent ferrate decay rate (Jiang et al., 2015). The drying procedure required for surface analyses may also impact particle characteristics; however, thermal transformation of iron hydr(oxides) generally requires higher temperatures (e.g., 200-400 C) than utilized in this study (Schwertmann and Cornell, 2008). Drying at 104C can lead to the transformation of $Fe(OH)_3$ to FeOOH through dehydration and crystallization (Cornell et al., 1989; Schwertmann and Cornell, 2008).

There are many factors and pathways in iron precipitation, and the precise mechanisms and structures of precipitates in some situations is not fully known (Duan and Gregory, 2003). Any proposed mechanistic differences between the precipitation of ferrate and ferric resultant solids carry some degree of speculation. Other work on the nature of

ferrate resultant particles have also determined the presence of Fe_2O_3 and FeOOH in a core-shell arrangement (Prucek et al., 2013). Results from this study confirm the presence of Fe_2O_3 in ferrate resultant particles through XPS analysis with a Fe $2p^{3/2}$ peak binding energy in close agreement with previous work. No attempt was made to quantify or describe possible core-shell arrangement.

2.5.2 Role of DOC, and Differences in Particle Characteristics

Dissolved organic carbon (DOC) plays an important role in the characteristics of particles resulting from ferrate and ferric iron addition in water. 99% of particles resulting from ferrate reduction in the laboratory water matrix (with no phosphate) were large particles. Comparatively, ferrate reduction in the natural water matrix led to a multimodal particle distribution with the overwhelming majority of iron existing as smaller particles.

The stabilizing impact of DOC on various types of particles has been well documented (Baalousha, 2009; Chen and Elimelech, 2007; Edzwald, 1993) and the observed similar impact on ferrate resultant particles is not especially noteworthy. Of greater interest is that the impact of DOC leads to significantly smaller particles in the case of ferrate reduction as compared to ferric hydrolysis. This result, combined with the differences in particle morphology, reinforce the possibility of differences between the processes that lead to particles from ferric addition (e.g., iron hydrolysis) and the process that leads to particles from ferrate reduction (e.g., direct crystallization or rapid aging).

Results indicate that a similar, relatively small fraction of DOC becomes associated with the surface of particles from both iron sources, and is removed during particle separation. The magnitude of this associated DOC is similar for both iron particle sources. The complexation of NOM at oxide interface has been well documented (Au et al., 1999; Gu et al., 1994; Vermeer et al., 1998); what is unique about these results is that a similar amount of NOM is associated with both particle types, despite the different particle characteristics. Future exploration of the specific surface area and crystal structure is required to more fully assess NOM association with ferrate resultant particles. Also, in the case of ferrate addition, NOM was subjected to oxidation, which was not the case for ferric iron addition. Oxidation can change the character of NOM, including partial destruction (Edwards and Benjamin, 1992; Gan et al., 2015; Jiang et al., 2006; Sharma et al., 2013), and this can both positively and negatively impact subsequent adsorption of NOM onto particle surfaces, depending on several factors (Bose and Reckhow, 2007; Edwards et al., 1994). No destruction of NOM was found based on the results in Figure 2.5. Results indicate that the effect of all of these factors yielded similar complexation of NOM onto the particle surfaces. The similar association of NOM on both ferrate and ferric resultant particles is likely the cause for the observed similar surface charges.

More examination must be conducted to elucidate the possible differences in particle formation processes. In this study, one pH value and one natural water were used from within a range common to drinking water treatment. No attempt was made to determine the effect of any individual water quality parameter on particle formation. NOM hydrophobicity and pH may play significant roles in the characteristics of particles resulting of ferrate reduction, and further examination is appropriate.

2.5.3 Implications for Water Treatment

The size and charge characteristics of iron particles resulting from ferrate reduction have important implications for the use of ferrate in drinking water treatment. An abundance of nanoparticles with negative surface charge would comprise a stable colloidal suspension and challenge downstream particle removal steps, possibly requiring additional coagulation. It is likely that this additional coagulation processes would not use ferrate as the iron source for a coagulant due to economic considerations, and more commonly used coagulants such as cationic polymers or more metal salts would be deployed. Therefore, ferrate may not ultimately serve the dual-role in drinking water treatment that had been previously anticipated, at least not in a manner that completely eliminates the need for a coagulation process step following pre-oxidation. Results of the charge titration indicate that the negative surface charge on ferrate resultant particles could be neutralized similarly to ferric resultant particles.

The nanoparticles resulting from ferrate reduction in natural water may also have positive impacts on water treatment objectives. The particles resulting from ferrate reduction in this study have much higher external surface area than a corresponding mass of ferric iron due to their smaller size, potentially leading to higher adsorption capacities and enhanced removal of common adsorbates such as arsenic (Prucek et al., 2013) or reduced manganese (Knocke et al., 1988). The smaller size could increase the reactivity of the particles and their efficacy in water treatment in ways yet to be determined. Examinations of the crystalline structure and specific surface area of ferrate resultant particles are required to inform potential adsorption processes.

The presence of phosphate buffers used in laboratory experiments clearly impacts the nature of particles resulting from ferrate reduction and is not representative of natural water chemistry. Iron fractionation results reinforce the potential for differences in the mechanisms of particle formation between the two iron types, and show differences in the sequestering effect of phosphate. There is some disagreement on the adsorption of phosphate onto an Fe surface (Lytle and Snoeyink, 2002); however, it is possible that differences in Fe(III) surfaces between the two resultant particle types affect reactions with phosphate. Different modifications to Fe(III) (hydr)oxides can lead to different reactivates, depending on surface coordination geometry (Stumm, 1992), and XPS results support differences in the crystalline structure between ferric and ferrate resultant particles. Increased phosphate removal with ferrate resultant particles as compared to ferric resultant particles has also been observed in a wastewater matrix (Lee et al., 2009). Reduction of ferrate in the phosphate buffer created a form of iron that passed through a 30 KDa UF membrane, operationally defined as dissolved. Future work could use different techniques for analysis of iron material, and more research should be conducted on the reductively inducted formation of Fe(III) from Fe(VI) to understand the impact of ligands.

Potential differences in precipitation mechanism between ferric and ferrate iron addition would have significant implications for water treatment. Prior research on ferrate has anticipated its use as an oxidant and coagulant; however, the effects of coagulants are not

a result of the nature of the simple aquo-metal themselves, but are dependent on the hydrolysis products (Stumm and O'Melia, 1968; Stumm et al., 1962). If iron that results from ferrate reduction in natural water does not undergo the same hydrolysis reactions as ferric chloride, then ferrate addition may not result in significant coagulation.

It is not appropriate to assume that the particles resulting from ferrate reduction are identical to particles resulting from the addition of a ferric coagulant in the context of water treatment, or that the processes that form the particles are the same. Studies aimed at the application of ferrate for water treatment should consider the unique characteristics of resulting particles when assessing the impact of ferrate addition on downstream treatment processes.

CHAPTER 3

OXIDATION OF MANGANESE(II) WITH FERRATE: STOICHIOMETRY, KINETICS, PARTICLES, AND IMPACT OF ORGANIC CARBON

Modified from originally submitted version (Goodwill, J.E., Mai, X., Jiang, Y., Reckhow, D.A., Gikonyo, J., Tobiason, J.E., Oxidation of Manganese(II) with Ferrate. Environ. Sci. Technol. In Review.)

3.1 Introduction

Manganese (Mn) is a contaminant of concern for many drinking water utilities. The negative impacts of Mn in drinking water are primarily aesthetic; however, some studies have noted potential health impacts in sensitive populations (Bouchard et al., 2011). Currently, the United States Environmental Protection Agency (USEPA) does not set a regulatory limit on Mn in drinking water, but has published a recommended secondary maximum contaminant limit (SMCL) of 0.05 mg/L. Chronic aesthetic problems can still occur at this SMCL, and so a typical treatment goal is approximately 0.02 mg/L (Kohl and Medlar, 2006). The USEPA has placed Mn on the 2015 Draft Contaminant Candidate List (CCL 4), and future regulation may be pending, forcing water utilities to reexamine their Mn control strategies.

Several treatment methods for removal of reduced, dissolved manganese (Mn(II)) are available, including oxidation followed by separation of the resulting particulate Mn oxide (Gregory and Carlson, 2003; Knocke et al., 1991; Reckhow et al., 1991; Sinsabaugh et al., 1986), adsorption onto Mn oxide coated granular media with subsequent surface oxidation (Coffey et al., 1993; Islam et al., 2010; Knocke et al., 2010; Tobiason et al., 2008), or biologically active filtration (Burger et al., 2008; Mouchet, 1992). The oxidation of dissolved Mn(II) typically requires strong oxidants such as ozone, chlorine dioxide or permanganate, as the kinetics of the oxidation of dissolved Mn(II) by free chlorine are slow at the typical pH range and time scales of drinking water treatment plants (DWTPs) (Sinsabaugh et al., 1986). The methods of manganese treatment have various advantages and disadvantages (Brandhuber et al., 2013).

The primary disadvantages of the oxidation of Mn(II) by strong oxidants includes relative operational complexity (e.g. production of oxidant and proper dosing), and the potential formation of disinfection byproducts (AWWA, 2011; Gordon et al., 1990; von Gunten, 2003; Werdehoff and Singer, 1987). Ferrate (Fe(VI)) is a potential alternative for pre-oxidation in drinking water treatment (Jiang and Lloyd, 2002; V. Sharma, 2002). The primary advantages of ferrate include a strong oxidation potential, disinfection properties (Sharma, 2007) and a lack of hazardous by-products (DeLuca et al., 1983). Fe(VI) has been shown to effectively oxidize reduced inorganics through single and multiple electron transfers (Sharma, 2011, 2010). Therefore, it is possible that Fe(VI) is a viable alternative for Mn(II) oxidation in drinking water treatment. However, there is a lack of research that examines the use of ferrate in treating manganese for drinking water.

The stoichiometry of Fe(VI) oxidation of Mn(II) remains unknown, which is an impediment to its use. Additionally, the rate of the reaction is unknown, as is the possibly competing role of other natural water solutes, such as natural organic matter (NOM). The characteristics of the subsequent iron and manganese particles that result from this reaction have also not been examined.

The objectives of this study were to: (1) quantify the stoichiometry of the oxidation-reduction reaction between Fe(VI) and Mn(II), and the possible competition from NOM; (2) evaluate the kinetics of the reaction relative to the typical time scale of drinking water treatment, and (3) examine the characteristics of resulting manganese and iron particles.

3.2 Materials and Methods

3.2.1 Water Quality

A deionized (DI) laboratory grade water with a 1 mM carbonate buffer was used in this study. NOM was added to the DI matrix in a subset of experiments. Two pH values of 6.2 and 7.5 and two Mn(II) concentrations of 5.5 and 10.9 μM (0.3 and 0.6 mg/L), ranges typically encountered in drinking water treatment systems, were utilized when assessing reaction stoichiometry. Manganous sulfate was the source of Mn(II). All experiments were conducted at 21 degrees Celsius.

3.2.2 Oxidation Reaction

The oxidation reaction was executed in batch reactors containing 750 mL of sample water. Fe(VI) was added to the solution during 60 seconds of rapid mixing ($G \sim 250\ sec^{-1}$).

Mixing intensity was then decreased (G ~ 60 sec^{-1}). pH was monitored and adjusted using 1M NaOH or 1M HCl, as needed.

Ferrate was added as a concentrated (2.5 mM FeO_4^{-2}) stock solution by dissolving potassium ferrate in DI water. The concentration of Fe(VI) was measured at the moment of addition via 510 nm wavelength light absorbance. A volume of the stock solution was immediately added to each reactor to yield the desired Fe(VI) concentration. The reaction time was forty-five minutes. The oxidation experiment was replicated at various ferrate dosages.

3.2.3 Kinetic Studies

Kinetic experiments were conducted using a rapid mixing stopped-flow unit (Applied Photophysics, RX2000) coupled with a diode array spectrophotometer with reverse optical geometry (Agilent, HP 8453). The minimum sampling interval of the spectrophotometer was 0.1 s, and the lag time of the stopped flow unit was 8 ms. The stopped flow unit injected sample from two syringes into a 1 cm path length quartz cell. One syringe contained a 225 μM Mn(II) solution in a 0.2 M borate buffer at pH 9.2 or 8.8 and the second syringe contained a 150 μM Fe(VI) solution, in a 1 mM borate, at pH 9.2 (dosing stoichiometric ratio was 2 mol Fe(VI): 3 mol Mn(II)). The strength of the Fe(VI) solution was immediately measured spectrophotometricaly using molar absorptivities of 1150 M^{-1} cm^{-1} and 1100 M^{-1} cm^{-1} at 510 nm for ferrate at pHs 9.2 and 8.8, respectively (Carr, 2008).

At the moment of mixing by the stopped-flow apparatus, the mixed solution pH was either 9.2 or 8.8. The decrease in absorbance at 510 nm was used to measure Fe(VI) concentration (e.g., direct measurement) (Lee et al., 2005a).

A numerical method was developed to estimate the second order reaction rate constant (k_2), based on the minimization of the root mean square error (RMSE) between measured Fe(VI) and numerical estimated values at each point. Results from the direct measurement of Fe(VI) were normalized with respect to the initial ferrate concentration, after the non-zero residual absorbance value were subtracted across all measurements. These normalized values were then compared to the model results to determine the RMSE.

3.3 Analytical Methods

3.3.1 Iron and Manganese Concentrations

Fe and Mn concentrations were measured in duplicate samples using an inductively coupled plasma mass spectrometer (ICP-MS), utilizing seven replicate measurements per sample. A third set of samples was analyzed by a colorimetric method (APHA et al., 2005). Results for the two measurement techniques were generally within 7% agreement. Results from the ICP-MS were used for reporting.

The absorbance spectrum of samples containing permanganate (Mn(VII)) was analyzed on a diode array, reverse optics spectrophotometer, using a quartz cell with a 10 cm path. Triplicate measurements were taken with each sample.

3.3.2 Particle Size

Particle size was characterized by fractionation with progressively smaller effective size exclusion filters, based on a method developed for Mn particles (Carlson et al., 1997). The filters used included a fine glass fiber (GF/F) filter with an effective size exclusion cut-off of 0.7 μm (GE Whatman), a polycarbonate microfiltration membrane filter (MF) with a pore-size of 0.2 μm (Nuclepore, Track-Etch Membrane, GE Whatman) and a regenerated cellulose ultra-filter (UF) membrane (EMD Millipore) with a molecular weight cut-off of 30 kDa. Solids not passing the GF/F filter were defined as large particles (LP). Solids passing the GF/F filter but not passing the 0.2 μm filter were defined as small particles (SP). Solids passing the 0.2 μm filter, but retained on the 30 kDa UF were defined as nanoparticles (NP), and metal passing the 30 kDa UF was operationally defined as dissolved. All resulting fractions from this technique are reported on a mass of metal basis.

3.3.3 Natural Organic Matter

NOM was measured as non-purgeable organic carbon (NPOC) using an organic carbon analyzer (Shimadzu TOC-VCPH). Dilutions of a 10 mg/L as C potassium hydrogen phthalate standard were used to calibrate the instrument. The samples were acidified with 6N HCl solution and purged with nitrogen before analysis. Multiple injections of duplicate samples were analyzed with the mean value and standard deviation of all

injections reported. Measurements generally conformed to Standard Methods Section 5310B (APHA et al., 2005). Results for organic matter were defined as total organic carbon (TOC) if analysis was conducted without prior sample filtration, and dissolved organic carbon (DOC) if analysis was conducted following filtration with a 30 kDa UF membrane.

3.3.4 X-ray Photoelectron Spectroscopy

X-ray photoelectron spectroscopy (XPS) was used to identify the oxidation state of Mn in particles using an adapted method developed for Mn solid surfaces in drinking water filtration media,(Cerrato et al., 2010) through careful observation of the position and shape of the Mn 3p photoline (Cerrato et al., 2011). XPS analysis was also conducted in Fe binding energy regions, with results compared to previous XPS analysis of ferrate resultant particles (Goodwill et al., 2015). Particles for XPS analysis were produced through the same experimental conditions as described for the oxidation study, but with a 3.5-liter reaction volume. Following reaction completion, the resulting particle solution was placed in a coagulant charge analyzer (CCA) (Chemtrac, CCA 3000), and in situ measurements were taken. The negative surface charge of the particles at pH 7.5 was titrated by drop wise addition of 1M H2SO4 while the solution pH and streaming current results were monitored (see Figure SI-1). At the point of zero charge (PZC), the solution was filtered through a GF/F filter which was then dried in a desiccator at 21 degrees Celsius. A portion of the filter was mounted onto carbon tape and subjected to XPS analysis. Powdered Mn and Fe oxide standards were mounted directly onto carbon tape.

Analysis was executed on a Phi Quantum 2000 spectrometer with a monochromatic Al Kα X-ray source operating at 1486.6 eV, 37.5 W. The beam diameter was approximately 200 μM. The pass energy was 23.50 eV, and the step size was 0.2 eV. XPS was also performed on an MnO_2 standard (Mn(VI) oxide, ≥99.9% purity, Alfa Aesar), a Mn_2O_3 standard (Mn(III) oxide, 99% purity, Strem Chemicals), a MnO standard (Mn(II) oxide, 99% purity, Strem Chemicals), and a α-Fe_2O_3 standard (Fe(III) oxide, ≥99% purity, Sigma Aldrich). The binding energy of all samples was charge referenced to the C1s peak at 285.0 eV. Intensities were normalized to facilitate direct comparison.

3.3.5 Reagents

Chemical reagents used were laboratory grade. The ferrate source was solid potassium ferrate (K_2FeO_4) with 92% purity (Sigma Aldrich). Hydrochloric acid (HCl), sodium hydroxide (NaOH), sodium bicarbonate ($NaHCO_3$) and Manganese(II) Sulfate ($MnSO_4$) were also obtained from Fisher Scientific. Natural organic matter was added as Suwannee River NOM Concentrate, RO Isolate (1R101N, IHSS). Sodium permanganate (NaMnO4) was obtained as a 40% by weight solution (Aldrich).

3.4 Results

3.4.1 Stoichiometry

Data for Mn(II) oxidation by Fe(VI) in buffered DI water are shown in Figure 3.1, including results for both pH values (6.2 and 7.5), and both initial manganese concentrations (0.3 mg/L and 0.6 mg/L), across a Fe(VI) dose range up to 7μM. Linear

regression of the data set produced a slope (a) of 0.67, with a standard error (SE) of 0.01. The 95% confidence interval for the slope is also shown, and includes the range between 0.65 and 0.69. The y-intercept (y_o) was set at 0 to reflect no Mn(II) oxidation at a zero Fe(VI) dose condition.

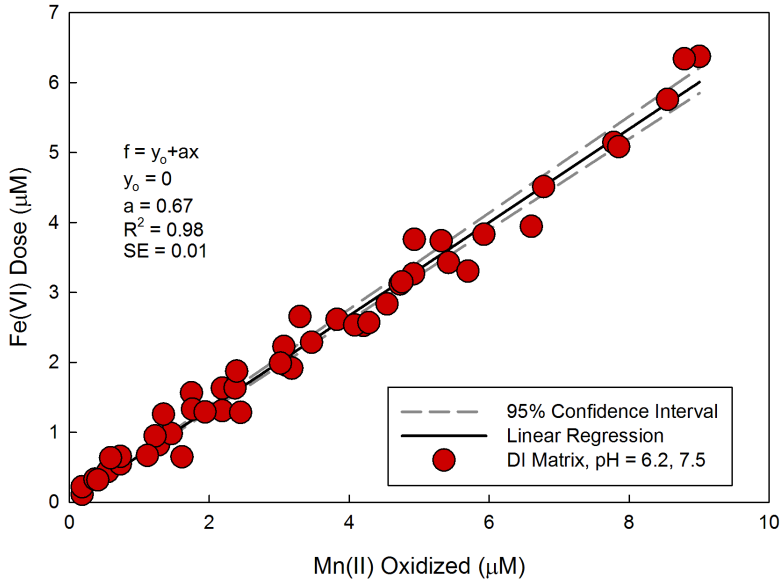

Figure 3.1 Linear relationship between Fe(VI) dose and Mn(II) oxidized in a laboratory water matrix; 1 mM HCO_3^-, pH = 7.5 and 6.2, $Mn(II)_i$ = 4.9 μM and 9.8 μM; N = 48

Results in Figure 3.1 indicate that the overall molar stoichiometry of the oxidation reaction between Fe(VI) and Mn(II) is 2:3, based on the slope of the linear regression. This molar ratio was constant for the two studied pH values and initial Mn(II) concentrations, with oxidation at both pH conditions yielding a slope of 0.67; the standard errors (SE) at pH 6.2 and 7.5 were 0.01 and 0.02, respectively.

Fe(VI) was also added in excess of the observed stoichiometric requirement corresponding to the selected initial Mn(II) level. In these cases, a persistent pink color was noted. Samples of this resulting solution were subjected to UF filtration and analyzed for spectrophotometric absorbance. Similarly, the absorbance of a $NaMnO_4$ solution was measured, with results for both solutions shown in Figure 3.2.

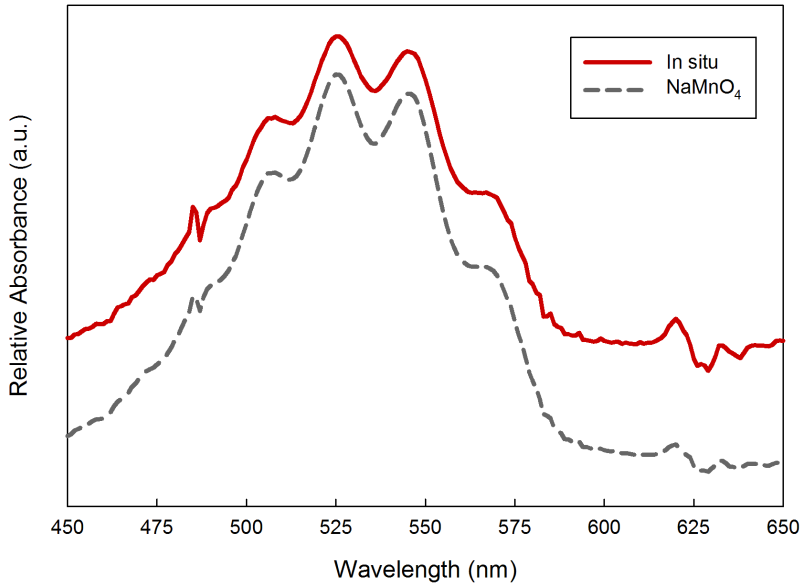

Figure 3.2 Relative absorbance of a super stoichiometric ferrate dose sample (e.g., in situ), and a MnO_4^- solution. In situ sample: DI water matrix; pH = 6.2; HCO_3^- = 1mM; $Mn(II)_i$ = 5.5 μM; Fe(VI) dose = 11 μM. NaMnO4 sample: pH = 6.2; HCO_3^- = 1 mM

Various super stoichiometric dosages of Fe(VI) were added to the DI matrix Mn(II) solution at pH values of 6.2 and 7.5. The absorbance at 525 nm was converted to μM as MnO_4^- using the corresponding molar absorptivity (ε = 2500 M^{-1} cm^{-1}). Figure 3.3 shows the concentration of Mn(VII) produced for approximate Fe(VI) to Mn(II) dosages of 1.3,

3.4 and 6.7, on a mole:mole basis. More Mn(VII) was formed as the ratio of Fe(VI) to Mn(II) increased. Also, oxidation at pH = 6.2 consistently produced more Mn(VII) than oxidation at pH 7.5. At pH 6.2, approximately 50% of the initial Mn(II) was converted to Mn(VII) at a mole Fe(VI) to mole Mn(II) ratio of 6.7, approximately 10 times the 0.67 mole Fe(VI) to mole Mn (II) stoichiometric requirement determined in the DI water matrix.

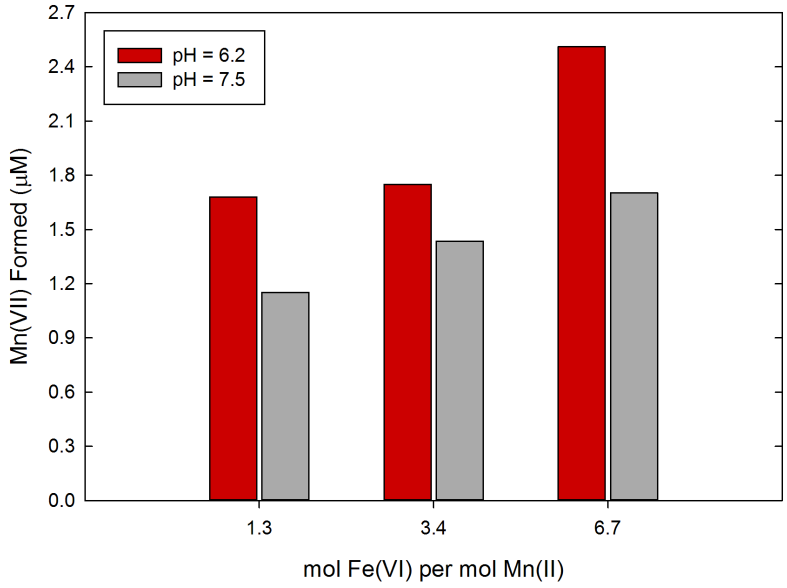

Figure 3.3 Mn(VII) formed during oxidation of Mn(II) with super stoichiometric dosages of Fe(VI). $Mn(II)_i$ = 4.9 μM; HCO_3^- = 1 mM

3.4.2 Reaction Kinetics

Ferrate decay versus time (60 second period) data for pH 9.2 and 8.8 for initial Mn(II) of 113 μM, and for ferrate only at pH 9.2 are shown in Figure 3.4. When no Mn(II) was present, the apparent Fe(VI) concentration decreased only slightly; however, when

Mn(II) was present, the Fe(VI) concentration decreased much more rapidly, indicating a reduction of Fe(VI) through Mn(II) oxidation. The apparent Fe(VI) concentration reached relatively constant, non-zero values at approximately 5 and 50 seconds for Mn(II) oxidation at pH 8.8 and 9.2, respectively.

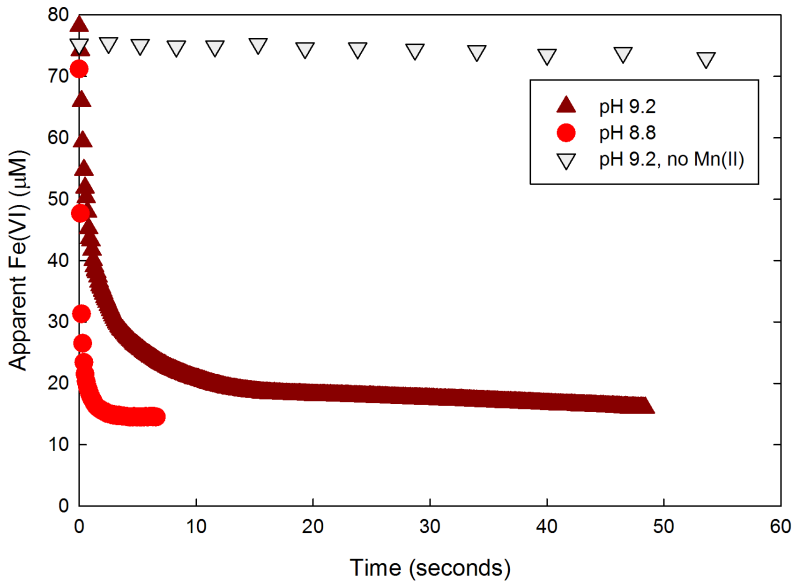

Figure 3.4 Apparent Fe(VI) concentrations during oxidation of dissolved Mn(II); BO_3^{-3} = 0.2 mM, pH as indicated, Fe(VI) initial = 75 μM, Mn(II) initial = 113 μM

The apparent non-zero steady-state concentrations were likely caused by light scattering from Mn and Fe solids and not residual Fe(VI). The use of phosphate for Fe and Mn particle sequestration was not possible due to the potential for precipitation of Mn-PO_4 prior to the oxidation reaction. Measurement of Fe(VI) concentrations using 2,2'-azino-bis(3-ethylbenzothiazoline-6-sulfonate (ABTS) (Lee et al., 2005a) was not possible due to ABTS oxidation by MnO_2 (Jiang et al., 2012).

It is clear from Figure 3.4 that the reaction between Mn(II) and Fe(VI) is very fast relative to the rate of ferrate decay in the absence of any oxidant demands. The estimated second order reaction rate constants at pH 9.2 and 8.8 were 1.0×10^4 M^{-1} s^{-1} and 5.6×10^4 M^{-1} s^{-1}, respectively. An example of the numerical model with normalized Fe(VI) decay measurements is included in the Appendix A (Figure A.5).

The oxidation reaction rate was found to be inversely proportional to pH, which has been noted for Fe(VI) oxidation of many other inorganics (Sharma, 2011). Fe(VI) decay for oxidation of Mn(II) at pH < 8.8 was too fast to be measured. Kinetic experiments in the presence of NOM were not successful, likely caused by the obscuring of absorbance by Fe(VI) at 510nm from a combination of particles and/or DOC. DOC in natural water has been shown to obscure direct ferrate decay measurements at 510 nm (Lee et al., 2005a).

3.4.3 Characterization of Resulting Particles

Particles resulting from the Fe(VI) oxidation reaction were analyzed using XPS, Results for the Mn 3p photoline are shown in Figure 3.5, including Mn(II) (i.e., MnO), Mn(III) (i.e., Mn_2O_3), and Mn(IV) (i.e., MnO_2), and oxidation resultant particles.

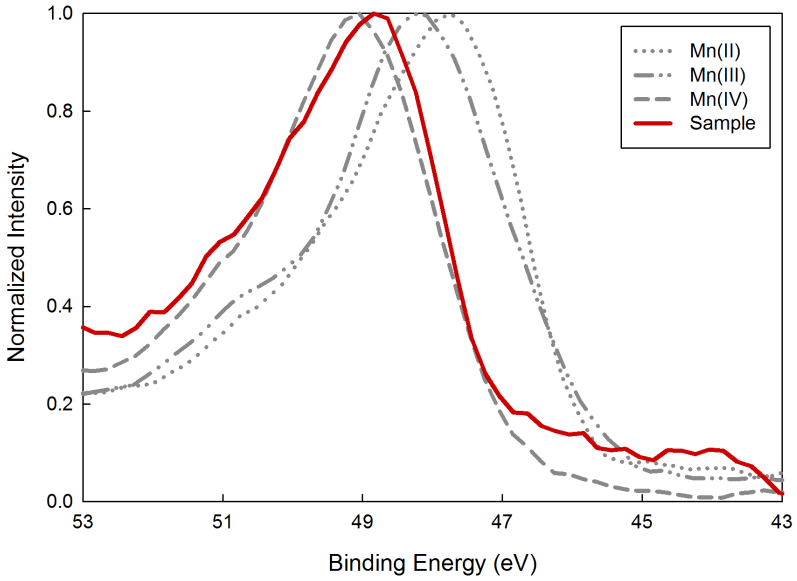

Figure 3.5 Mn 3p (7P) photoline spectrum for Mn oxide standards and particles resulting from Mn(II) oxidation by Fe(VI). For oxidation reaction, pH = 7.5, HCO_3^- = 1 mM

The Mn 3p peaks for Mn(II), Mn(III) and Mn(IV) occurred at binding energies of 47.7 eV, 48.3 eV, and 49.1 eV, respectively, in close agreement with similar analyses on the same manganese oxides (Cerrato et al., 2011). The oxidation resultant particles had an Mn 3p peak at 48.9 eV, more similar to MnO_2 than the other Mn standards, supporting the conclusion that Mn(IV) is the product of Mn(II) oxidation by Fe(VI).

XPS was also executed on resultant particles in the Fe $2p^{3/2}$ region, and compared to an α-Fe_2O_3 standard and particles resulting from ferrate reduction in the absence of any other oxidant demands (Goodwill et al., 2015) (see Appendix A, Figure A.6). In general, Fe in particles resulting from Mn(II) oxidation by Fe(VI) had photoelectron spectra similar to

the α-Fe_2O_3 standard and to particles resulting from Fe(VI) reduction alone; binding energy peak locations were 711.0 eV, 710.9 eV, and 711.0 eV, respectively.

The size fractionations of Mn and Fe solids formed in the oxidation reaction are shown in Figure 3.6. Fractionation was conducted on a sample that received an approximate stoichiometric dose of 0.67 mole Fe(VI) to 1 mole Mn(II) in both water matrices and studied pH values. Figure 3.6 shows that dosing Fe(VI) at the stoichiometric level for complete Mn(II) oxidation yields 99% and 93% oxidized Mn particles in the DI water matrix at pH 6.2 and 7.5, respectively. This is generally consistent with the linear relationship demonstrated in Figure 3.1. However, the size distribution of Fe and Mn particles formed vary between the pH values, with oxidation at pH 6.2 yielding approximately 80% small particles (SP) for both Fe and Mn, on a mg of metal basis. At pH 7.5, the majority of Fe and Mn solids were nanoparticles (NP). This was similar to the particle size distribution for the water containing NOM.

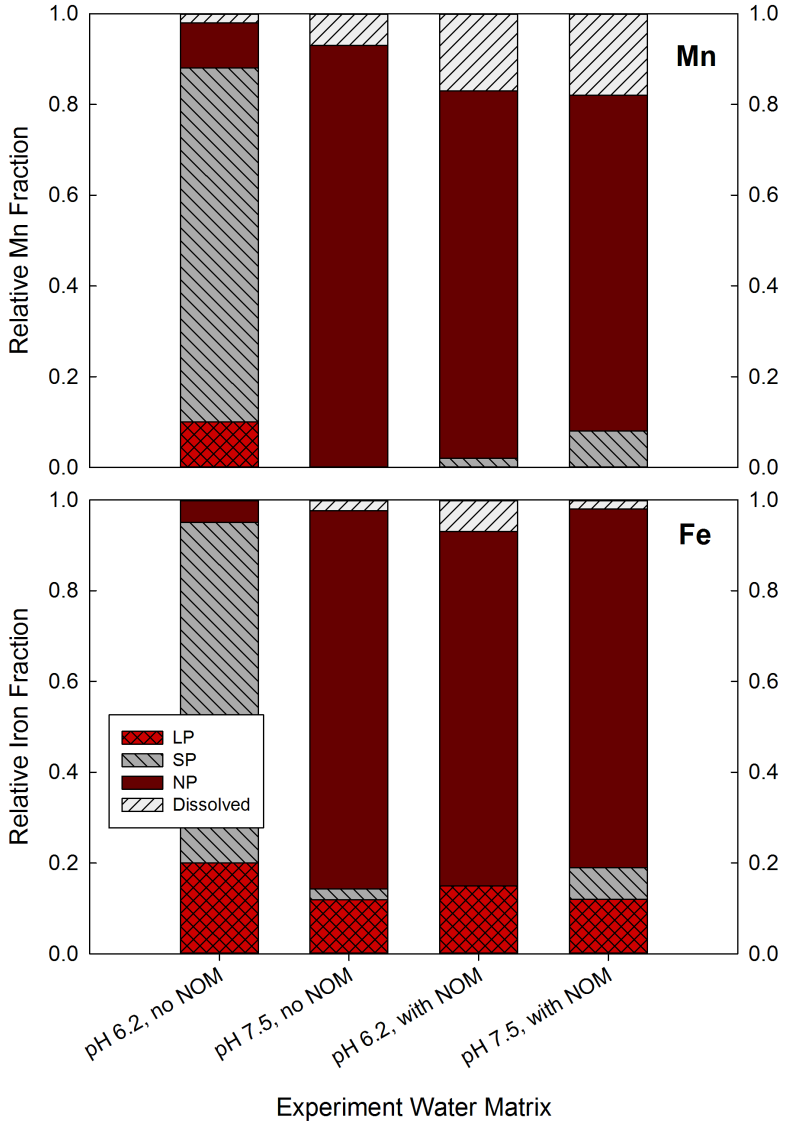

Figure 3.6 Size fractionation of iron and manganese particles resulting from oxidation of Mn(II) with Fe(VI), on a mass of metal basis. In samples with NOM, TOC = 1.75 mg/L, DOC = 1.5 mg/L. HCO_3^- = 1 mM; $Mn(II)_i$ = 4.9 μM; Fe(VI) = 3.3 μM (LP = Large Particles, SP = Small Particles, NP = Nanoparticles).

3.4.4 Impact of NOM

The Mn(II) oxidation experiments were repeated with laboratory water spiked with NOM, yielding total organic carbon (TOC) and dissolved organic carbon (DOC) levels of approximately 1.75 and 1.5 mg/L, respectively. Figure 3.7 includes results for both pH values, as well as a line showing the observed stoichiometry for the no NOM DI water experiments.

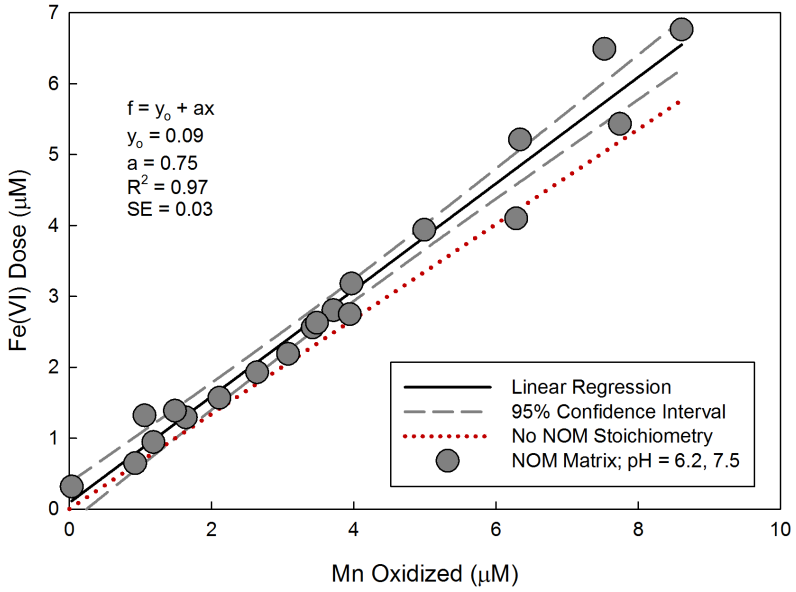

Figure 3.7 Linear relationship between Fe(VI) dose and Mn(II) oxidized in deionized water matrix with natural organic matter; TOC = 1.75 mg/L; 1 mM HCO_3^-, pH = 7.5 and 6.2, $Mn(II)_i$ = 4.9 μM and 9.8 μM; N = 19

The slope of the linear regression line for the NOM matrix Mn oxidation was 0.75, with a 95% confidence interval ranging from 0.69 to 0.81. It should be noted that the lower band of the 95% confidence interval, 0.69, is equal to the upper band of the 95% confidence interval of the DI water matrix slope.

The linear regression of the NOM results was not forced through the origin, allowing for ferrate dosages that yielded no Mn(II) oxidation. The y-intercept (yo) of the linear regression line was 0.09; however, the 95% confidence interval for yo included 0, indicating the potential for no initial ferrate demand. There was not a significant difference between the slopes and y-intercepts between the two studied pH values in the NOM matrix, similar to the results for the DI water matrix. Details of the linear regression for both water matrices and pH values are included in Table A.2 in Appendix A.

The presence of NOM also impacted the particle size distribution of resulting particles. In the NOM water matrix, at both pH values, the overwhelming majority of Fe and Mn particles were nanoparticles, on a mass of metal basis (see Figure 3.6).

The fate of NOM following Fe(VI) addition was assessed through the fractionation of TOC and DOC of the solution resulting from the oxidation reaction, across various Fe(VI) dosages at the two studied pH values (see Appendix A, Figure A.7). In general, the TOC levels are unchanged while Fe(VI) dose increased, indicating negligible amounts of organic carbon mineralization as a result of Fe(VI) oxidation. At pH 7.5, the level of DOC was also relatively unchanged as Fe(VI) dose increased, in contrast to pH 6.2, where DOC decreased by approximately 50% following oxidation at a Fe(VI) dose of 0.68 mole Fe(VI) per mole Mn(II).

3.5 Discussion

3.5.1 Reaction Stoichiometry and Kinetics

The stoichiometry of the Mn(II) oxidation by Fe(VI) can be approximated at 2 mol Fe(VI) to 3 mol Mn(II), based on the linear relationship in Figure 3.1, for solutions without other oxidant demands (eq. 3.1).

$$2Fe(VI) + 3Mn(II) \rightarrow 2Fe(III) + 3Mn(IV) \qquad \text{(eq. 3.1)}$$

A major implication of the stoichiometry presented in Equation 3.11 is that Fe(VI) undergoes a net three electron gain to Fe(III) during oxidation of Mn(II) to Mn(IV), resulting in Fe(III) and Mn(IV). In other oxidation reactions, ferrate(VI) may undergo a one or two electron transfer resulting in perferryl(V) or ferryl(IV) (Sharma, 2011, 2010), much more reactive compounds which may react indiscriminately and/or self-decay, ultimately producing Fe(III) (Lee et al., 2014). The net three electron transfer per mole of Fe(VI) for oxidation of Mn(II) is similar to the oxidation of other inorganic contaminants by ferrate such as As(III) to As(V) (Lee et al., 2003).

The addition of Fe(VI) above the stoichiometric requirement for Mn(II) created Mn(VII) in a DI water matrix. This phenomena has also been noted with ozone (Netzer et al., 1973). There are two probable options for the stoichiometry of Mn(VII) formation from

oxidation of Mn species by Fe(VI), one involving Mn(II) (eq 3.2), and the other involving Mn(IV) (eq. 3.3).

$$5Fe(VI) + 3Mn(II) \rightarrow 5Fe(III) + 3Mn(VII) \qquad \text{(eq. 3.2)}$$

$$Fe(VI) + Mn(IV) \rightarrow Fe(III) + Mn(VII) \qquad \text{(eq. 3.3)}$$

The observed Mn(VII) production shown in Figure 3.3 was significantly lower than either Equation 3.2 or Equation 3.3 would predict, based on the amount of Fe(VI) added. In one experiment, 6.7 mole of Fe(VI) was added per mole of Mn(II), yet only approximately 50% of the initial Mn(II) was converted to Mn(VII), at a pH of 6.2. This indicates that not all electrons involved in reducing Fe(VI) to Fe(III) in this situation came from Mn. The other primary source of electrons would be H_2O or reduced iron.

The increase in Mn(VII) formation as oxidation pH decreases can be attributed to the pH dependent nature of the oxidation potential of Fe(VI) (V. Sharma, 2002). The formation of Mn(VII) during Mn(II) oxidation with Fe(VI) could cause significant issues in drinking water treatment, including aesthetic problems related to a persistent pink color, and precipitation of MnO_2 in distribution systems and plumbing fixtures as a result of Mn(VII) reduction over time. Mn(VII) may also interact with filter media following pre-oxidation, and form or regenerate a manganese oxide coating on the granular media (Islam et al., 2010; Merkle et al., 1997; Tobiason et al., 2008).

Results from evaluation of reaction kinetics indicate that the oxidation of Mn(II) by Fe(VI) is very fast (e.g., complete in << 60 seconds) relative to the typical time range utilized in pre-oxidation in drinking water treatment (e.g., several to thirty minutes) (AWWA and ASCE, 1998). The estimated second-order rate constants were 1.0×10^4 M^{-1} sec^{-1} and 5.6×10^4 M^{-1} sec^{-1}, at pH 9.2 and 8.8, respectively. In comparison, the second order rate constant for Fe(VI) oxidation of As(III) at pH 9 is 2×10^4 M^{-1} sec^{-1} (Lee et al., 2003). The rate constant values for Mn(II) oxidation by Fe(VI) are greater than for Fe(VI) oxidation of other inorganic contaminants including iodide and cyanide at similar pH values (Sharma, 2010). The second order rate constant values at neutral pH for Mn(II) oxidation by O_3, ClO_2 and MnO_4^- have been determined by others to be 2×10^4, 1×10^4 and 1×10^5 M^{-1} sec^{-1}, respectively (Knocke et al., 1991; Reckhow et al., 1991). The results for ferrate oxidation in this study, and the impact of pH, suggest that ferrate oxidation of Mn(II) at neutral pH is faster than the other strong oxidants. The rate of Fe(VI) decay in the presence of Mn(II), even at relatively high pH values studied, was much faster than Fe(VI) decay in natural water matrices without Mn(II) (Jiang et al., 2015). Therefore, the rate of the reaction indicates that application of Fe(VI) for Mn(II) oxidation in a pre-oxidation (e.g., before coagulation) step will be effective with reaction completion well in advance of downstream particle destabilization, aggregation and separation processes. The rate of Mn(II) oxidation by Fe(VI) increased as pH decreases, which is the inverse of what has been noted for Mn(II) oxidation by other oxidants (Knocke et al., 1991). This is attributable to the oxidation potential of ferrate increasing as pH decreases (Wood, 1958).

The method chosen to evaluate kinetics (i.e., direct spectrophotometric determination of Fe(VI)) was utilized based on the limitations of other methods, and is likely impacted by resultant particles. Therefore, reported reaction rate constants should be considered estimates. The oxidation of Mn(II) by Fe(VI) at typical pH conditions is clearly fast relative to pH conditions and time scales typically used in water treatment.

3.5.2 Particle Characteristics

The size distribution of particles resulting from Mn(II) oxidation by Fe(VI) varied with respect to pH, with oxidation at pH 6.2 yielding mostly SPs and oxidation at pH 7.5 yielding mostly NPs. Other strong oxidants, such as ozone and permanganate, have also been noted to form NPs from Mn(II) (Brandhuber et al., 2013). The mean particle size for mixed Mn(IV) and Fe(III) particles was smaller than the mean size of Fe(III) particles resulting from Fe(VI) decay in the absence of other oxidant demands in a similar DI water matrix (Goodwill et al., 2015). The mixed Mn and Fe particles also had negative surface charges as determined by streaming current measurements (see Figure A.1.).

3.5.3 Impact of NOM

DOC was found to exhibit a Fe(VI) demand that competed with Mn(II). However, the overall effect was relatively small, as indicated by the slight change in slope of the linear regression line shown in Figure 3.2, and the negligible change in TOC resulting from Fe(VI) addition in Figure A.7. This implies that Mn(II) oxidation by Fe(VI) may still be effective in water with moderate amounts of NOM co-occurring with Mn(II). Evaluations of Mn(II) oxidation by ozone have also noted much less inhibition from humic material as compared to oxidation of Fe(II) (Reckhow et al., 1991).

Results of TOC analysis indicate no appreciable mineralization of NOM as a result of Fe(VI) oxidation in the presence of Mn(II), However, at pH 6.2, approximately 50% of DOC was removed across a UF membrane, suggesting adsorption of DOC onto the Fe/Mn oxide particle surface and subsequent removal via particle separation, or direct precipitation by Fe(III). Much more DOC was removed at pH 6.2 as compared to pH 7.5; this pH effect has been noted previously for adsorption of organic material by Mn and Fe oxides (Tipping and Heaton, 1983; Tipping, 1981). Different NOM concentrations and characteristics could have different impacts on the oxidation of Mn(II) by Fe(VI). Further study of the oxidation reaction between Mn(II) and Fe(VI) in various NOM contexts is appropriate.

3.5.4 Implications for Drinking Water Treatment

Results indicate that ferrate may be a very effective alternative to other strong oxidants typically used for Mn(II) oxidation in drinking water treatment. The reaction between Mn(II) and Fe(VI) occurs very rapidly, and is not significantly impacted by competition from low amounts of NOM co-occurring with Mn(II). DWTPs utilizing Fe(VI) for Mn(II) treatment will need to limit overdosing Fe(VI) above the stoichiometric ratio determined in this work to prevent the formation of Mn(VII). The relatively small particles with negative surface charges resulting from Mn(II) oxidation by Fe(VI) can have impacts on the downstream particle removal processes in drinking water treatment. For example, at pH 7.5, oxidation of Mn(II) yielded approximately 90% of resultant Mn and Fe as nanoparticles, which would likely require additional destabilization and/or

aggregation prior to removal. It is unlikely that additional Fe(VI) would be added for this particle destabilization step due to economic considerations, the likelihood of producing Mn(VII), and the lack of hydrolysis processes for ferrate resultant particles (Goodwill et al., 2015). Assuming adequate removal of formed particles, NOM removal via association with metal oxide surfaces may be realized.

CHAPTER 4

LABORATORY ASSESSMENT OF FERRATE FOR DRINKING WATER TREATMENT

Modified from originally submitted version (Goodwill, J.E., Mai, X., Jiang, Y., Reckhow, D.A., Gikonyo, J., Tobiason, J.E., Laboratory Assessment of Ferrate For Drinking Water Treatment. Journal American Water Works Association. In Review.)

4.1 Introduction

Ferrate (Fe(VI)) has been proposed as a viable alternative to other strong oxidants such as chlorine dioxide, ozone and permanganate as used in drinking water treatment (DWT) (Jiang and Lloyd, 2002; Sharma et al., 2005). As a strong oxidant, there has been much published research on the oxidation of various inorganic and organic contaminants by Fe(VI). Generally, Fe(VI) effectively and rapidly oxidizes contaminants germane to water treatment, relative to typical dosages of iron (Fe) and process time-scales. Additionally, ferrate has been evaluated as a coagulant with respect to removal of turbidity (Ma and Liu, 2002a), formation of flocs (Graham et al., 2010), and interactions with natural organic matter (Jiang and Wang, 2003; Lim and Kim, 2009), as compared to traditional coagulants (e.g. salts of iron and aluminum). Contradiction in the literature exists, with some researchers concluding ferrate improved the removal of organics during coagulation, and others finding little or no impact. Fundamental processes have not been discussed in great detail. Ferrate has been demonstrated to inactivate various pathogens (Gombos et al., 2012; Hu et al., 2008; Sharma, 2007) at exposure values that appear

achievable in water treatment (Jiang et al., 2015). Ferrate does not form hazardous byproducts (DeLuca et al., 1983).

Ferrate can be produced by several methods including oxidation by chlorine in an alkaline solution (e.g., wet oxidation method) (Ockerman and Schreyer, 1951), and electrochemically (Alsheyab et al., 2009). Following production via wet oxidation or electrochemical methods, the product can be refined through a process involving potassium hydroxide, precipitation and drying, ultimately yielding >95% purity potassium ferrate (K_2FeO_4) (Thompson et al., 1951). A version of these processes has been commercialized by the Battelle Memorial Institute (Monzyk et al., 2013). Also, a version of the wet oxidation method has been commercialized by Ferrate Treatment Technologies (Ciampi and Daly, 2009). This technology currently produces ferrate that has been used successfully in several applications including the treatment of industrial wastewater and ship ballast water. Due to the use of chlorine in this manufacturing process, chlorine may be present in the final ferrate product, potentially leading to the formation of chlorinated byproducts in treated water, especially in the case of preoxidation (e.g., the addition of an oxidant to raw water). Therefore, to avoid the potential formation of disinfection byproducts (DBPs), it is possible that dosing the potassium ferrate salt (K_2FeO_4) will be the most common ferrate adaptation for drinking water treatment. Issues related to using K_2FeO_4 include shipping and dosing of a solid product. K_2FeO_4 was used for all batch and continuous flow experiments in this work.

The most commonly considered application of ferrate in drinking water treatment is as a preoxidant—occurring before the primary particle removal step. This is because of the formation of Fe(III) solids that results from Fe(VI) reduction, and the expectation that these particles are best formed prior to particle destabilization (e.g., coagulation) and separation (i.e., clarification and/or filtration) processes.

In the absence of specific oxidant demands, ferrate undergoes automatic decomposition (i.e., auto decay) that includes the oxidation of water, and the formation of Fe(III) solids and hydrogen peroxide (Carr, 2008; Lee et al., 2014). In a natural water matrix, natural organic matter (NOM) or buffer systems (e.g., carbonate) may serve to stabilize ferrate decomposition, likely through complexation with Fe(III) solids that would otherwise catalyze Fe(VI) decay (Jiang et al., 2015). Natural sources of drinking water may also contain discrete oxidant demands such as reduced metals, organic contaminants, and pathogens. Thus, ferrate is likely to react through multiple simultaneous pathways when added to raw water as a preoxidant, with the oxidized constituents potentially playing a role in subsequent treatment processes.

As shown in Figure 1.2, the possible impacts of adding ferrate to a raw water are multiple and complex. Very few studies have focused on the impacts of adding ferrate for drinking water treatment in a manner that accounts for multiple possible outcomes. Also, very few studies have evaluated the use of ferrate in continuous flow (e.g., pilot) experiments in a drinking water context, and the full impact of adding ferrate, both on water quality and

downstream physical-chemical processes is not fully known. Therefore, the objectives of this study are: (1) conduct batch experiments to evaluate the impact of adding ferrate as a preoxidant on subsequent coagulation (2) conduct continuous flow experiments to evaluate the impact of adding ferrate as a preoxidant on downstream physical and chemical water treatment processes, and water quality; (3) comment on the general benefits and feasibility of using ferrate in drinking water treatment as compared to other treatment chemicals such as permanganate (MnO_4^-) and ferric chloride ($FeCl_3$).

4.2 Materials and Methods

4.2.1 Batch Experiments

The batch experiment protocol is shown in

Figure 4.1. Raw water of various sources was buffered with 10 mM borate, and ferrate was added as a preoxidant directly as a K_2FeO_4 salt, under rapid mixing at room temperature (21 deg C). Ferrate concentrations were measured using an indirect indicator spectrophotometric method (Lee et al., 2005a). Two ferrate dosing conditions were utilized: a lower dose of 25 μM and a higher dose of 50 μM, which were chosen based on preliminary experiments (Goodwill et al., 2014). Fe(VI) preoxidation was conducted at two pH values, 6.2 and 7.5, to span the range of pH values commonly encountered in drinking water treatment. Following at least 45 minutes of reaction time, a portion of the resultant solution was analyzed for various parameters, while the remainder was subjected to coagulation.

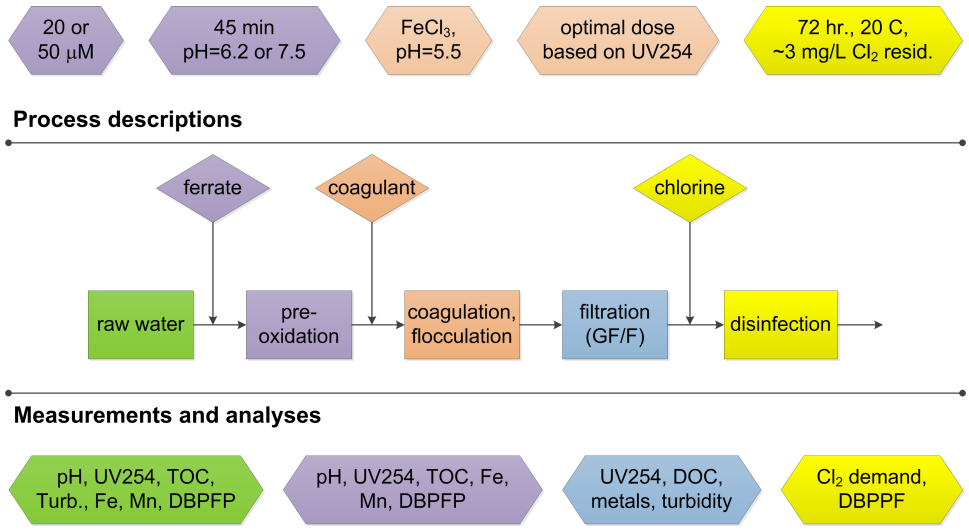

Figure 4.1. Batch experimental method diagram; UV254=absorbance of ultra-violet light at 254 nm, GF/F=glass fiber fine, TOC=total dissolved carbon, DOC=dissolved organic carbon, DBPFP=disinfection byproduct formation potential

Coagulation was executed based on a common jar test procedure (Hudson and Wagner, 1981). Jar tests were executed using a programmable flocculator (Kemwater, Kemira). Six samples (e.g. jars) were dosed with various amounts of ferric chloride under rapid mixing (G ~ 200 sec^{-1}), followed by 10 minutes of slower mixing (G ~ 50 sec^{-1}). The pH was controlled at 5.5 by drop wise addition of 1 M NaOH or 1M HCl, as required. Following flocculation, the solution was allowed to settle under quiescent conditions for 30 minutes. Then, a 20 mL sample was taken from the reactor and filtered using a fine glass fiber filter (Whatman GF/F) with an effective size exclusion of 0.7 μm. The UV254 absorbance of each jar test sample was measured, and the Fe(III) dose that yielded the lowest value of UV254 absorbance was defined as the optimum ferric dose (OFD). If

ferric coagulant dosages yielded the same (e.g. < 5% difference) UV254 absorbance, then the lower of the two dosages was defined as the OFD. Optimal coagulation was defined by UV254 absorbance based on the nature of the raw waters (e.g., surface waters, relatively low turbidity, relatively high UV254 absorbance), consistent with typical practice of coagulation controlled by organic demand (Edzwald, 1993; Edzwald and Tobiason, 1999). UV254 absorbance was chosen as the primary measurement parameter because it is an excellent surrogate parameter for estimating concentrations of organic carbon in natural water (Edzwald et al., 1985).

4.2.2 Continuous Flow Experiments

The treatment processes were developed to replicate full-scale DWT systems. The full-scale facilities chosen for this study used a packaged water treatment plant currently sold by WesTech (Trident®). The major characteristics of the Trident System include the use of an up-flow roughing filter, known as an adsorption clarifier (AC), filled with relatively coarse (2-3 mm in diameter), low-density plastic media in place of a more conventional gravity based clarifier. The continuous flow system was constructed using PVC pipe, NSF 61 certified for use with potable water. Prior to coagulation and clarification, Fe(VI) was dosed as a concentrated (1 mM) solution, proceeded by approximately 40 minutes of ferrate contact time through a series of two continuous flow stirred tank reactors. The Fe(VI) stock solution was made by dissolving K_2FeO_4 of 97% purity (Battelle Corporation) in deionized water. Following this preoxidation step, coagulants and pH control chemicals were added to replicate full-scale systems immediately prior to an in-line static mixer (see details in Table 4.2). Water then flowed to the up-flow AC and then down through a conventional anthracite (15 inches) over sand (9 inches) dual-media filter.

Filter media were collected from a full scale treatment facility using the Trident Package Plant system in a manner explained elsewhere (Islam et al., 2010; Soucie et al., 2003). The hydraulic loading rates of the AC and media filter were 20 and 10 m/hr, respectively. Headloss was monitored across the dual media filter. Turbidity and UV254 measurements were taken every minute following filtration using on-line flow through instrumentation. pH was also measured at various points across the treatment systems and was adjusted as necessary following preoxidation to replicate full scale conditions (see Table 4.2).

Two experiments were conducted for each source water, one without ferrate, replicating full-scale conditions (i.e., coagulant type, coagulation pH, etc.) and then a second with ferrate, keeping other factors the same. This allowed for a direct evaluation of the impact of adding ferrate to the treatment process train.

In a subset of continuous flow experiments, preoxidation with Fe(VI) was compared to preoxidation using Mn(VII), and to the addition of Fe(III) as $FeCl_3$ prior to the primary coagulation step. In the case of Mn(VII), a dose was chosen to reflect the dose used at the full-scale facility. The $FeCl_3$ dose was chosen to yield the same concentration of iron as the K_2FeO_4 dose (~3 mg/L as Fe). $FeCl_3$ was added in the same location as the preoxidants. Following the contact tank, pH was adjusted using NaOH to replicate the pH of coagulation of the full-scale treatment systems prior to rapid mixing.

4.2.3 Analytical Methods—Batch Experiments

UV254 absorbance was measured using an ultraviolet and visible light spectrophotometer with forward optics (Genesys 10S, Thermo Scientific). All samples for UV254 absorbance measurement were filtered with a GF/F filter prior to measurement of the absorbance of 254 nm wavelength light in a 1 cm path length quartz cell. Turbidity was measured using a laboratory turbidimeter that met the reporting requirements of EPA Method 180.1 (2100N, HACH). Iron, chlorine, and manganese concentrations were measured using adapted colorimetric methods (APHA et al., 2005), and a colorimeter (DR2400, HACH). Alkalinity was also measured colorimetrically via titration (APHA et al., 2005).

4.2.4 Analytical Methods—Continuous Flow Experiments

UV254 absorbance at the media filter effluent was measured using a flow through, online spectrometer (Spectrolyzer, S::CAN) at two minute increments. Turbidity was measured using a laboratory turbidimeter (Ratio XR, HACH) with a flow through cell apparatus. Headloss across the dual media filter was recorded using pressure transducers (Series 200, Noshok). The pH meters, turbidimeter, and pressure transducers were connected to a 14-bit analog to USB data acquisition device (USB-1408FS, Measurement Computing), which logged results to a computer every 30 seconds. Particle counts were measured in four predefined size channels using a light blockage instrument (2400PS, Chemtrac), operated in flow through mode (100 mL/min). Particle count data were streamed directly to a computer with measurements recorded every 30 seconds.

4.2.5 Analytical Methods—Organic Carbon and DBPs

For samples from both the batch and continuous flow experiments, organic carbon was quantified through measurements of non-purgeable organic carbon (NPOC) with a Shimadzu TOC-VCPH carbon analyzer. A hydrogen phthalate standard (10 mg/L) was used to calibrate the instrument. All samples were acidified with 6 N HCl and purged with nitrogen prior to analysis. OC measurements conformed to Standard Methods Section 5310B (APHA et al., 2005).

Measurement of disinfection byproduct formation potential (DBPFP) was initiated by chlorinating buffered (pH = 7.0, 10 mM phosphate) samples in 300 mL chlorine demand free, headspace free bottles, and incubated at 20 deg C for 72 hours. Chlorine dosages were as required to yield a residual between 3 and 5 mg/L as Cl2 following the incubation period. After incubation the samples were analyzed for four trihalomethanes (THMs) and nine haloacetic acids (HAAs). THMs were measured by liquid/liquid extraction with pentane followed by gas chromatography (GC) with electron capture detection (ECD), and conformed to USEPA Method 551.1. HAAs were measured by liquid/liquid extraction with methyl-tertiary-butyl-ether (MTBE), deriviatization with acidic methanol and analysis by GC-ECD. The HAAs analysis method conformed to USEPA Method 552.2.

4.2.6 Source Waters

Waters used in the batch experiments were collected from eleven different surface water sources across New England. In general, the water collected was typical of surface waters

in the northeastern part of the United States: low hardness, low turbidity, with moderate to high amounts of dissolved organic matter. None of the studied water sources had appreciable concentrations of inorganic contaminants such as iron, manganese or arsenic. Thus, the focus of preoxidation was on the removal of organic matter and minimizing DBP formation potential. Table 4.1 includes water quality information for the studied waters.

Table 4.1. Water quality information for all batch experiment water; OFD = optimal ferric chloride dose, SUVA = specific ultra-violet absorbance

Sample Name	TOC mg/L	DOC mg/L	UV254 Abs 1/cm	SUVA L/mg/m	OFD mg/L as Fe	Raw pH
Atkins	3.3	3.1	0.09	2.9	6	7.1
Catamount	5.9	5.2	0.22	4.1	12	6.6
Holton	6.4	5.8	0.11	1.8	10	7.0
Stockbridge	2.9	2.7	0.08	2.9	4	6.6
Northampton	1.7	1.5	0.06	4.0	5	6.5
Norwalk (in)	3.3	3.2	0.14	4.3	10	7.2
Norwalk (meso)	4.4	4.3	0.16	3.7	11	6.5
Norwalk (hypo)	2.8	2.8	0.11	3.8	11	6.5
Palmer	2.0	2.0	0.04	2.1	4	6.5
Readsboro	2.0	2.0	0.12	6.0	4	6.0
South Deerfield	2.1	2.1	0.08	3.6	6	7.0

Two water sources were selected from the set of waters used in the batch experiments for continuous flow experiments: Atkins and South Deerfield. More information about the treatment parameters for these two waters is included in Table 4.2.

Table 4.2. Full scale and continuous flow experimental parameters

Treatment Parameter	Atkins	S. Deerfield
Coag. Type	Cationic Polymer (Nalco 8100)	Cationic Polymer (Chemtrade EC-461)
Coag. Dose mg/L as product	6.9	5.9
Full-scale preoxidation	No	Mn(VII) Seasonally
Coag. pH	6.9	7.5
Ferrate Dose μM	25	50
Filter Run Time hours	8	8

4.3 Results

4.3.1 Batch experiments

The results for UV254 absorbance following coagulation at the OFD with and without ferrate preoxidation at various dosage and pH values are shown in Figure 4.2. In four cases, ferrate preoxidation yielded lower UV254 absorbance following coagulation than coagulation alone (Holton, Readsboro, South Deerfield and Stockbridge). In general, this benefit was more pronounced when preoxidation occurred at a pH of 6.2 than at 7.5. However, for the majority of studied waters, coagulation with Fe(VI) preoxidation did not have an appreciable impact on removal of UV254 absorbance as compared to only coagulation with $FeCl_3$. A similar effect has been noted for assessing the impact of ferrate peroxidation on the formation of disinfection byproducts following chlorination (Jiang et al, Submitted). Ferrate preoxidation did not generally change the OFD of waters

following ferrate preoxidation, as shown in Table 4.2 For the Catamount, Northampton and Stockbridge waters, however, the OFD decreased 16%, 40% and 33%, respectively.

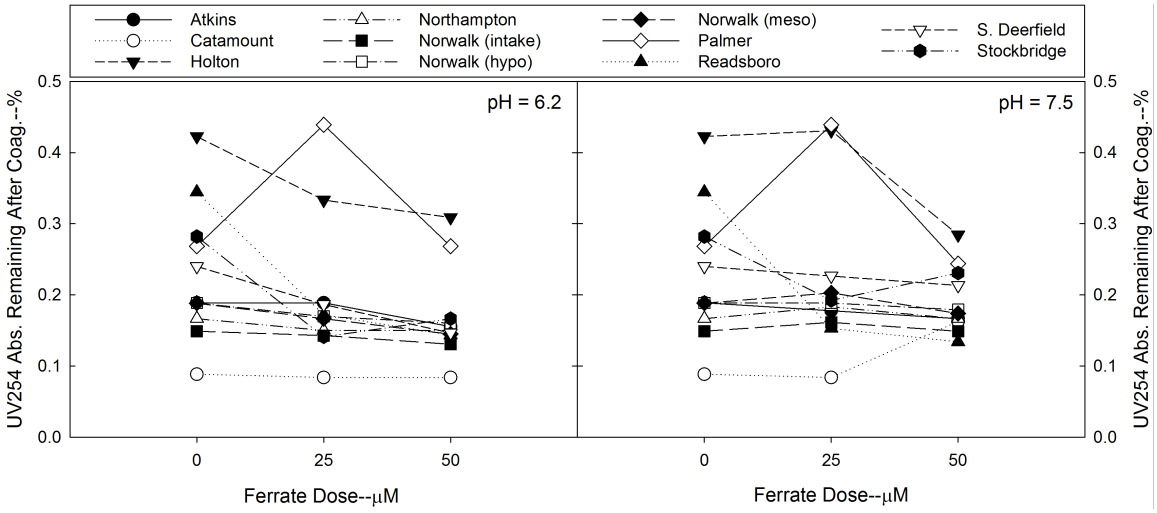

Figure 4.2. UV254 absorbance following coagulation at optimum $FeCl_3$ dose with and without ferrate preoxidation; coagulation pH = 5.5, borate buffer = 1 mM

Table 4.3. Optimal ferric dose with and without ferrate preoxidation; coagulation pH = 5.5

Utility	Optimal Ferric Dose--mg/L				
	No Ferrate	25uM, pH=6.2	25 uM, pH=7.5	50 uM, pH=6.2	50 uM, pH=7.5
Atkins	6	5	6	6	6
Catamount	12	10	10	10	10
Holton	10	9	10	10	9
Northampton	5	4	4	3	5
Norwalk (intake)	11	11	11	11	11
Norwalk (hypo)	11	11	11	11	11
Norwalk (meso)	10	10	10	10	10
Palmer	4	4	4	3	3
Readsboro	4	4	4	3	4
South Deerfield	6	6	6	6	6
Stockbridge	6	4	4	5	5

4.3.2 Continuous flow experiments

The impact of ferrate preoxidation on UV254 absorbance removal by downstream processes was examined using continuous flow experiments. Dual media filter effluent UV254 absorbance was monitored in parallel with turbidity and filter headloss, with results shown in Figure 4.3. Turbidity for both studied waters shows decreasing trends initially that can be attributed to filter ripening. Following establishment of steady performance, the UV254 absorbance for the Atkins water with and without Fe(VI) preoxidation was approximately 0.050 and 0.045 cm^{-1}, respectively, indicating approximately a 10% decrease in UV254 absorbance as a result of preoxidation as compared to no preoxidation. Likewise, for South Deerfield, the UV254 absorbance with and without Fe(VI) preoxidation was approximately 0.028 and 0.022 cm^{-1}, respectively, approximately a 20% decrease as a result of preoxidation

The continuous flow experimental results for turbidity show a similar pattern as UV254 absorbance, with lower turbidities resulting from ferrate preoxidation. For the Atkins water, turbidity with and without ferrate preoxidation was 0.22 and 0.12 NTU, respectively, and for South Deerfield, turbidity with and without ferrate preoxidation was 0.09 and 0.08 NTU, respectively. The relative improvement in turbidity was more significant for the Atkins water.

The removal of more turbidity and UV254 absorbance did not correlate with an increase in headloss across the dual media filter. Results shown in Figure 4.3 have been referenced

to the initial clean bead headloss, and are in units of inches of H_2O. In general, headloss development across the dual media filters for both waters with and without ferrate was very low due to the prior clarification process; however, headloss for both waters with preoxidation increased fairly quickly over the first hour of operation, and then much more gradually as operation continued. Ultimately, headloss results for both waters and preoxidation conditions were very similar. The addition of ferrate preoxidation did not negatively affect the ability of the AC or dual media filter to successfully operate for the desired filter run length.

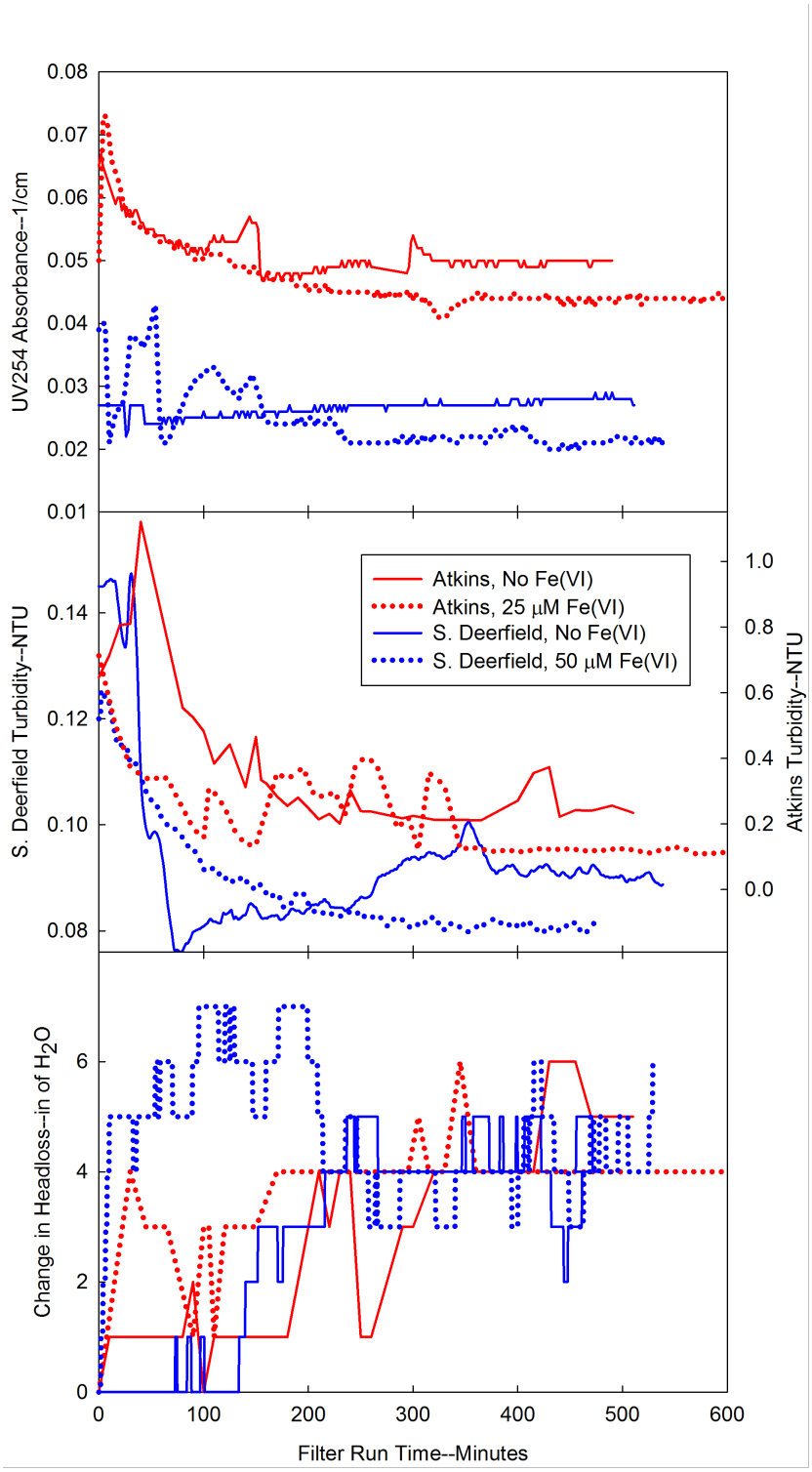

Figure 4.3. UV254 absorbance, turbidity and headloss results from continuous flow experiments

The impact of Fe(VI) on filter performance was also assessed through particle counts in the filter effluent, with results shown in Figure 4.4. Particle count measurements were only made during the South Deerfield experiment. In general, particle counts with and without ferrate were low and within typical treatment goals. Ferrate preoxidation resulted in 3-5 particles per mL, while no preoxidation yielded filter effluent particle counts of approximately 30 per mL. Particle counts generally agree with turbidity results in Figure 4.3. Results indicate no negative impacts of ferrate preoxidation in terms of particles in filter effluent. It should be noted that the minimum detectable particle diameter of the light blockage counting instrument was 2 μm, and the maximum detectable diameter is 100 μm. Attempts at measuring particles number concentrations using dynamic light scattering (DLS) were not successful, likely due to insufficient particle concentration in the filtered effluent.

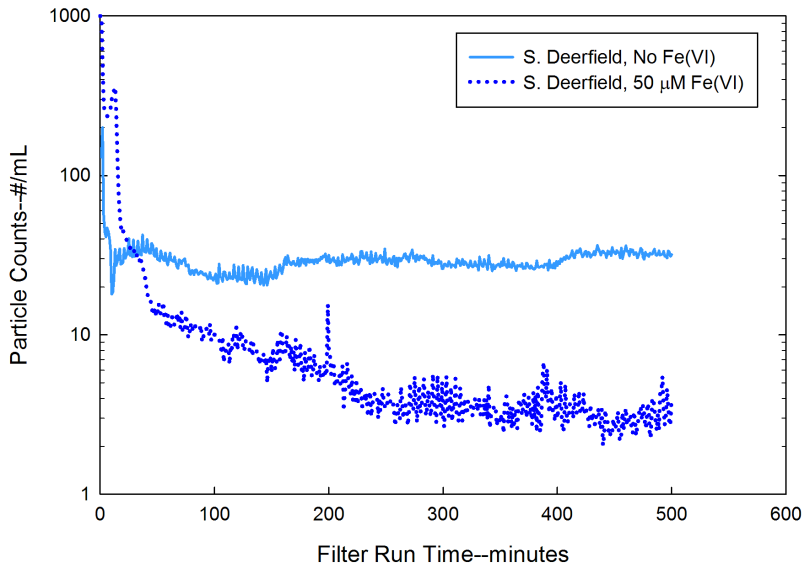

Figure 4.4. Counts of particles between 2 μm and 100 μm in diameter from light-blockage instrument in filter effluent with and without ferrate preoxidation

The primary source of particles from ferrate addition is reduction of Fe(VI) to Fe(III). The fate of iron contributed by ferrate was examined across the treatment system with results shown in Figure 4.5. Figure 4.5 shows the increase in iron concentration as a result of ferrate addition. In the inlet of the oxidant contact tank (CT), the iron concentration was approximately 2.9 mg/L, with approximately 90% of the iron defined as dissolved, on a mass of metal basis. Following coagulation and rapid mixing, almost all iron was particulate, with a total iron concentration of 2.5 mg/L. Approximately 90% of iron was removed across the AC. Following filtration, the iron concentration was < 0.1 mg/L, well below the United States Environmental Protection Agency (USEPA) Secondary Maximum Contaminant Level (SMCL) of 0.3 mg/L.

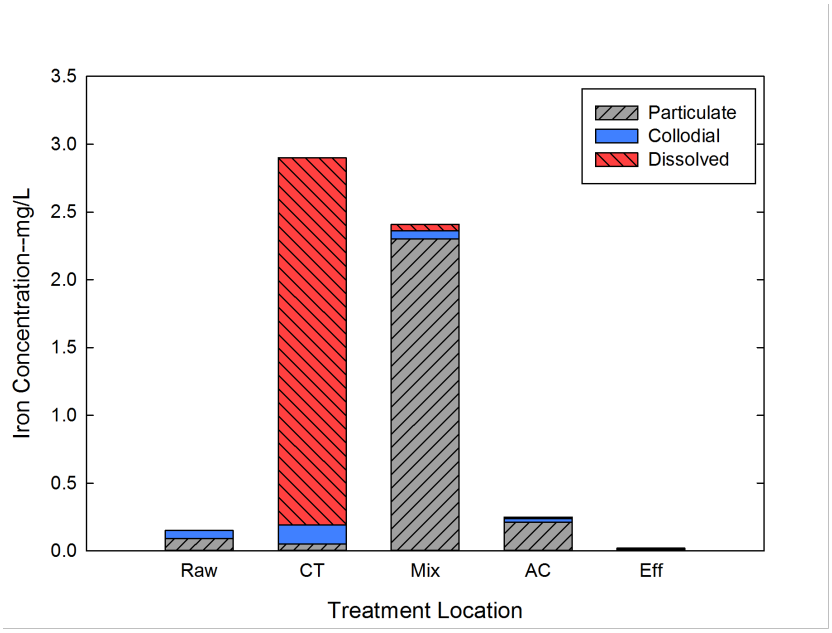

Figure 4.5. Profile of iron concentrations and fractions across continuous flow experiment processes for South Deerfield water with ferrate preoxidation; CT = contact tank, Mix = following addition of coagulant, pH control and rapid mixing, AC = adsorption clarifier, Eff = filter effluent; Fe(VI) dose = 50 μm

Results of disinfection byproduct formation potential analysis following filtration and chlorination for continuous flow experiments are shown in Figure 4.6. Also included are results for DBPFP after previously un-chlorinated finished water from the full-scale facilities was subjected to the previously described chlorination procedure. Results for DBPFP at the full scale are similar to results for the respective continuous flow experiments. Concentrations of THMFP and HAAFP for the experiments using Atkins water were greater than those for the South Deerfield water. This coincides with results of UV254 absorbance for the continuous flow experiments, which showed greater UV254 absorbance remaining in Atkins water than in the South Deerfield water. For the Atkins water, THMFP and HAAFP levels decreased from approximately 105 μg/L to 90 μg/L. as a result of preoxidation with ferrate. A decrease in DBPFP was also noted for the South Deerfield samples, but to a lesser extent, even though the dose of Fe(VI) was two-times that used for the Atkins water (25 μM versus 50 μM). Variations in Fe(VI) impact on DBPFP across variations in water quality has also been noted in batch experiments (Jiang et al., Submitted).

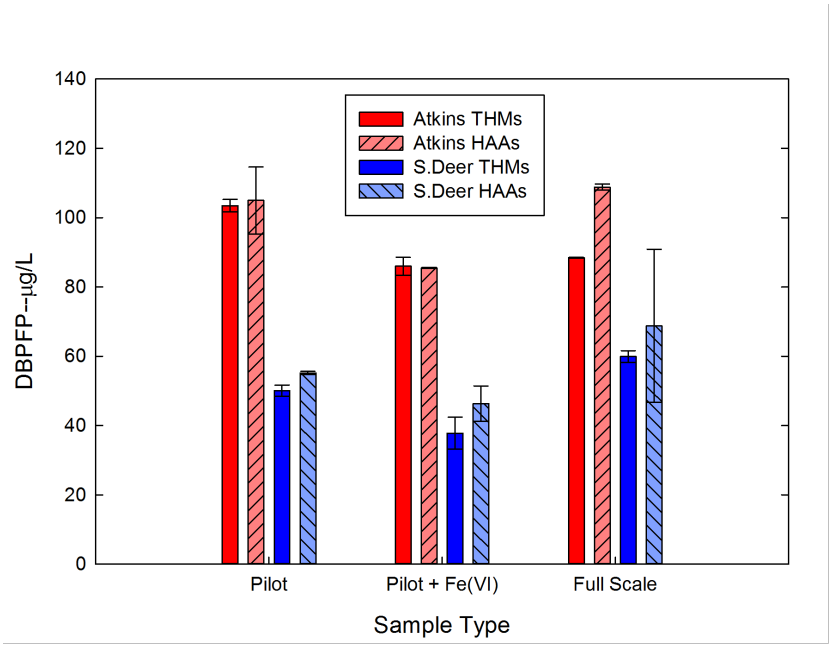

Figure 4.6. Continuous flow and full scale disinfection byproduct formation potential results for Atkins and South Deerfield water; For Atkins, Fe(VI)= 25 μM, For South Deerfield, Fe(VI)=50 μM

Continuous flow experiments were repeated twice on South Deerfield water, once using Mn(VII) preoxidation, and once using Fe(III) addition (at the same dose as Fe as the ferrate peroxidation case) to allow for direct comparisons to ferrate preoxidation, with results for UV254 absorbance and turbidity shown in Figure 4.7. Ferrate preoxidation yielded lower turbidity and UV254 values compared to no preoxidation (e.g., polymer only), or preoxidation with Mn(VII). However, results for UV254 absorbance and turbidity were very similar for Fe(III) addition and Fe(VI) preoxidation. The Fe(III) and Fe(VI) dosages were both approximately 3 mg/L as Fe. Thus, results indicate that the benefits of lower turbidity and UV254 absorbance following clarification and filtration are likely a function of ferric iron, and not due to the oxidative effect of Fe(VI).

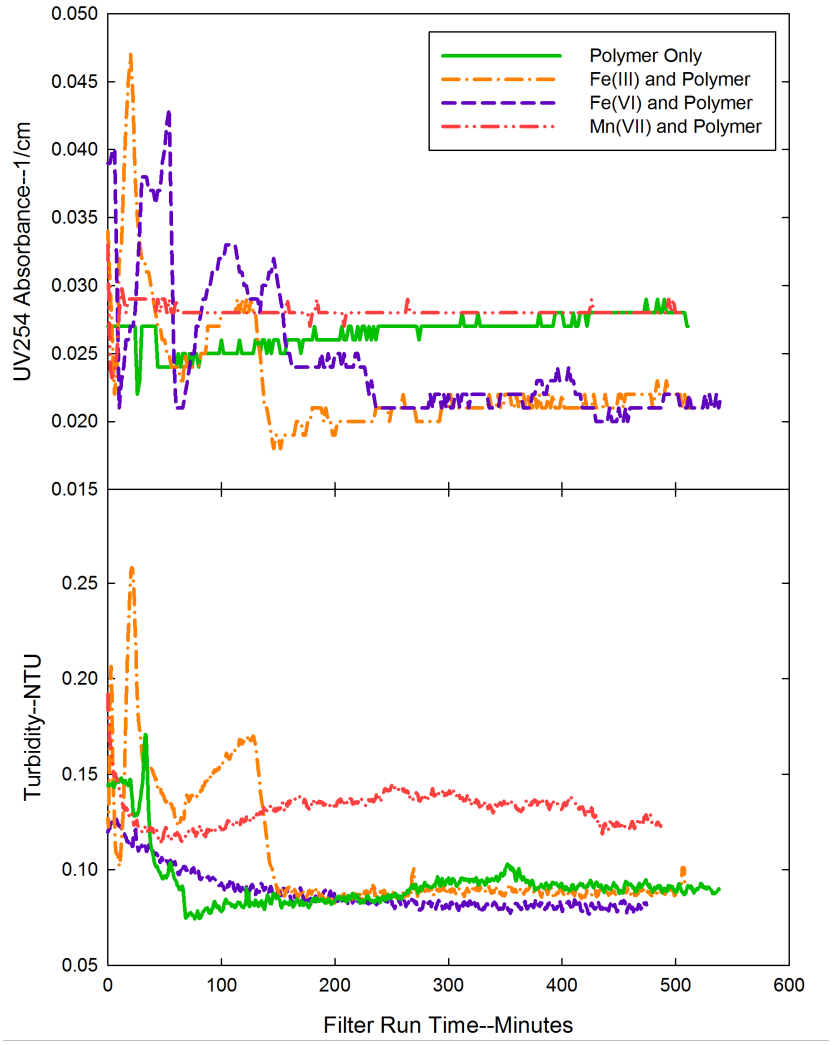

Figure 4.7. UV254 absorbance and turbidity results for continuous flow experiments on South Deerfield water utilizing no preoxidation (Polymer Only), Fe(III) and Polymer, Fe(VI) and Polymer, and Mn(VII) and Polymer; Fe(III) = 3 mg/L as Fe, Fe(VI) = 50 μM (2.9 mg/L as Fe), Mn(VII) = 10 μM

The performance in continuous flow experiments for Fe(VI), Fe(III) and Mn(VII) were also compared with respect to DBPFP with results shown in Figure 4.8. Results support UV254 absorbance and turbidity results, with water treated with Fe(VI) and Fe(III)

having similar levels of THMFP and HAAFP, which were both lower than THMFP and HAAFP in water treated with Mn(VII) or without any preoxidation. For the no preoxidation and preoxidation with Mn(VII) cases, the THMFP was approximately 50 μg/L and the HAAFP ranged from 55 to 60 μg/L. For the Fe(III) and preoxidation with Fe(VI) case, the THMFP was approximately 40 μg/L. Fe(III) treatment produced 39 μg/L of HAAFP while Fe(VI) preoxidation produced 50 μg/L.

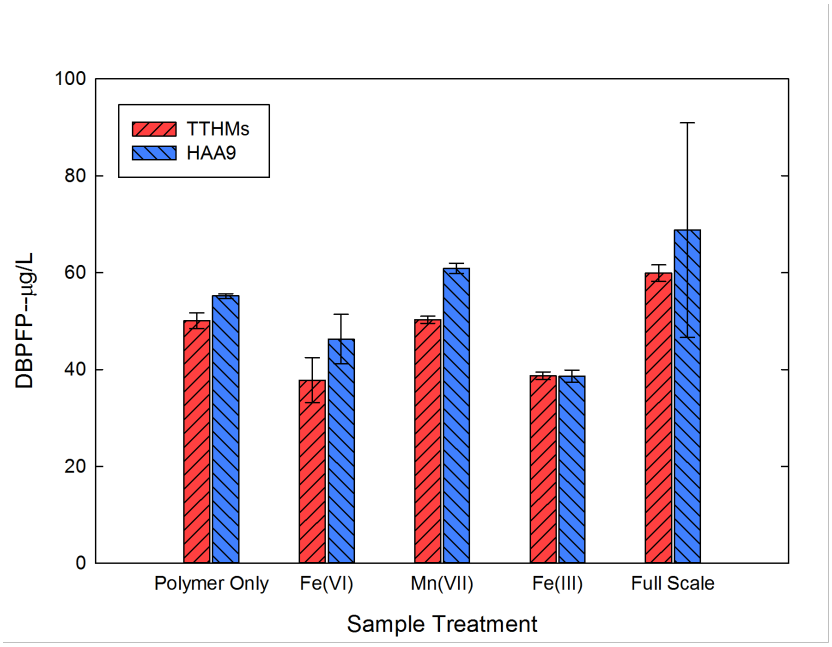

Figure 4.8. Disinfection byproduct formation potential results for continuous flow experiments on South Deerfield water; Polymer= 6 mg/L as product, Fe(VI) = 50 μM (2.9 mg/L as Fe), Mn(VII)=10 μM, Fe(III) = 3 mg/L as Fe

4.4 Discussion

4.4.1 Ferrate and coagulation—batch experiments

The UV254 absorbance results for the batch experiments indicate that Fe(VI) preoxidation had a modest impact on subsequent coagulation aimed at the removal of humic substances when compared to coagulation with $FeCl_3$ without any preoxidation. In some instances, preoxidation with Fe(VI) improved removal of UV254 absorbance, but in the majority of instances it did not. Preoxidation with ferrate did not lead to significant decreases in the OFD in most of the studied water samples. The variability in Fe(VI) effect is likely attributable to variations in the natural organic matter properties, as pH and mixing conditions were held constant across all batch experiments. The variable effect of ferrate on coagulation has been noted by other researchers, and has been attributed to the oxidation effects of ferrate on organic matter, including the cleaving of more humic macromolecular structures into more hydrophilic structures (Graham et al., 2010). The cleaving of organic structures has also been understood to occur following preoxidation with ozone (Edwards et al., 1994; O'Melia et al., 1999).

In the batch experiments, when Fe(VI) did improve UV254 absorbance removal after subsequent coagulation, the benefit was generally greater when preoxidation occurred at pH 6.2 versus 7.5. However, ferrate decay in natural water is highly dependent on pH, with the rate of decay decreasing as pH increases (Jiang et al., 2015). Therefore, UV254 absorbance removal increased even as ferrate exposure (i.e.., dose × time) decreased. One possible explanation is the increase in oxidation potential of Fe(VI) as pH decreases (Carr

et al., 1984). Alternatively, results point to a more complex relationship between Fe(VI) and reduction byproducts Fe(V) and Fe(IV) that are known to form from ferrate decay (Lee et al., 2014; Sharma et al., 2005). Ferryl(IV) and perferryl(V) are potentially reactive with numerous oxidant demands (Sharma, 2010; Sharma et al., 2005; V. K. Sharma, 2002), and half-lives of the two species are very short, making spectrophotometric measurement difficult (Lee et al., 2005a). It is possible that Fe(V) and Fe(IV) play an important role in NOM removal through preoxidation and subsequent coagulation, which would be independent of pH, and more pronounced as Fe(VI) decays into more reduced forms of iron.

4.4.2 Ferrate and filtered water quality—continuous flow experiments

For the two continuous flow experiments conducted on Atkins and South Deerfield water, preoxidation with ferrate generally improved finished water quality as compared to no preoxidation. Results indicate that, for both treatment systems, finished water quality resulting from full-scale treatment simulation could be improved by the addition of Fe(VI). Preoxidation with Fe(VI) lead to lower filtered water turbidities and UV254 absorbance values, without impacting filter run times. Fe(VI) preoxidation also lead to decreases in DBP formation potential.

The successful coagulation and ultimate removal of particulate iron is noteworthy, as previous studies had indicated that Fe(VI) reduction in natural water leads to large fractions of stable nanoscale particles that could challenge downstream particle removal

processes (Goodwill et al., 2015). Results from this study demonstrate successful destabilization of particles resulting from ferrate reduction by coagulation with subsequent removal via clarification and dual media filtration. Lower turbidities resulting from ferrate preoxidation followed by coagulation have also been previously noted (Ma and Liu, 2002a).

The improvement in finished water quality resulting from ferrate was also more significant than the impact of preoxidation with Mn(VII). However, Fe(VI) preoxidation did not improve finished water quality more than adding the same mass dose of Fe(III). The addition of Fe(III) lowered UV254 absorbance and turbidity to similar levels as compared to Fe(VI), and decreased the formation of HAAs approximately 15% more than for Fe(VI) preoxidation. These results are important as they imply that much if not all of the benefit from adding Fe(VI) in the South Deerfield water could be realized simply by adding the same amount of Fe(III) prior to the existing coagulation process. While meaningful cost data do not exist for ferrate in full-scale drinking water treatment, it is very likely that ferric coagulants represent a lower cost treatment option than ferrate (ferric coagulants are one of the inputs for commercialized wet oxidation ferrate manufacturing systems). Therefore, at least in the specific case of the South Deerfield water, ferrate does not represent the most viable option for improving turbidity, removal of organics and regulated disinfection byproducts. There are numerous other water quality objectives that were not explored under the scope of this work that are likely to require a strong oxidant such as ferrate as $FeCl_3$ addition alone would not be effective. Potential examples include the oxidation of dissolved manganese (Goodwill et al.,

Submitted), inactivation of pathogens (Gilbert et al., 1976; Hu et al., 2008), and the removal of algae (Ma and Liu, 2002b), Microcystin (W. Jiang et al., 2014) and arsenic (Lee et al., 2003). It is also possible that Fe(VI) preoxidation would lead to different outcomes as compared to Fe(III) with water containing organic matter with different characteristics than the water in this study.

4.4.3 Engineering and operational considerations

Evaluation of ferrate through continuous flow experiments afforded the opportunity to assess possible engineering or operational issues that would arise from adding ferrate preoxidation to an existing drinking water treatment system. The addition of ferrate did not appreciably impact headloss across dual media filters following clarification by an upflow adsorption clarifier. Results from the iron profile indicate that the majority of iron resulting from ferrate reduction was removed by the clarification process prior to filtration. Headloss measurements across the AC were not made; however, during piloting of the South Deerfield and Atkins treatment facilities, headloss development across the AC was very low (e.g., inches of H_2O after several hours of operation). In general, headloss development across the dual media filters both with and without ferrate preoxidation in these continuous flow experiments followed the headloss development profile and magnitude of the respective pilot facilities (Dumais, 1990; Norgren et al., 1993). Irrespective of headloss development, the addition of Fe(VI) will lead to the need to removed addition mass of iron residual solids across a treatment system.

Consistent ferrate dosing was achieved by dissolving K_2FeO_4 into DI water and dosing a concentrated solution. At larger scales, Fe(VI) can be added as a solution, or as a powder, perhaps in a manner similar to calcium hypochlorite. If Fe(VI) is added as a solution of K_2FeO_4, then ferrate stability will need to be considered. In this study, ferrate was found to be stable for several hours when a concentrated solution was made in DI water (pH ~ 9.2). At the full scale, it is likely that ferrate solutions will be made with finished water, due to economic considerations. Ferrate decay in this water matrix may be different than DI water, and should be evaluated prior to the use of ferrate at the full scale. Alternatively, ferrate can be produced on site via the wet oxidation method, assuming no residual chlorine is present in the final product, and the very high pH and conductivity of the resulting ferrate solution is not prohibitive. There has also been piloting for in situ electrochemical production of Fe(VI) for wastewater treatment (Yates et al., 2014).

Ferrate exists in several protonated states in aqueous solutions (Sharma, 2011) and thus increases the pH of an aqueous solution when added as a potassium salt of the conjugate base. In the continuous flow experiments, pH was found to increase following the addition of ferrate, and the addition of acid during coagulation was needed to achieve the desired operating pH representative of existing full-scale conditions. In some situations, the possibility of pH control will be a factor to consider for ferrate in drinking water treatment, especially if the ferrate solution generated is a very alkaline solution.

CHAPTER 5

CONCLUSIONS

This study made important findings that will impact the potential use of ferrate in drinking water treatment.

The presence of natural organic matter greatly impacts the size and surface charge of particles resulting from ferrate reduction. In laboratory water at pH = 6.2 with no dissolved organic carbon or phosphate, ferrate reduction yields relatively large (> 1 μm) particles, with a zeta potential of approximately -5 mV; in the study water with DOC ~ 3 mg/L, the majority of particles had diameter less than 200 nm, and a zeta potential of approximately -25 mV.

Natural organic matter associates with ferrate resultant particles in a similar manner as with ferric resultant particles. The association of natural organic matter to both ferrate and ferric resultant particle surfaces is likely the cause for similar surface charge between the two particle types in the studied natural water matrix.

The presence of phosphate during ferrate reduction has a major impact on resulting iron particles that is not representative of what occurs in natural waters. Additionally, differences in particle formation between ferric and ferrate iron in the presence of

phosphate point to potential differences in the mechanisms of particle formation for ferric versus ferrate iron addition.

There are significant differences in the size and morphology between iron particles resulting from ferrate reduction and particles resulting from ferric iron hydrolysis in natural water. Compared to ferric chloride addition, when ferrate is applied to natural water, the resulting particles have a much smaller average size, and a more granular, smoother morphology.

It is not appropriate to assume that the particles resulting from ferrate reduction are similar to particles resulting from the addition of a ferric coagulant, in the context of water treatment, or that the processes that form the particles are the same. Studies aimed at the application of ferrate for drinking water treatment should consider the unique characteristics of resulting particles when assessing the impact of ferrate addition on downstream water treatment processes.

In the laboratory water matrix without NOM, the oxidation of Mn(II) by Fe(VI) was found to follow a stoichiometry of 2 moles Fe(VI) to 3 moles Mn(II), resulting in reduced, particulate Fe(III) and oxidized, particulate Mn(IV). The size distribution of resulting particles included significant amounts of nanoparticles. The observed stoichiometric ratio held for multiple initial Mn(II) concentrations and pH values. The presence of NOM did

not significantly affect the stoichiometry, indicating limited competitive oxidant demand. Fe(VI) dosages above the stoichiometric ratio produced Mn(VII). The rate of the Mn(II) oxidation reaction was fast relative to typical time scales in drinking water treatment, with an estimated second order rate constant of approximately 1.0×10^4 M^{-1} s^{-1} at pH 9.2.

In batch experiments involving numerous raw water samples, preoxidation by Fe(VI) was found to have varied impact on UV254 absorbance removal with subsequent coagulation. In the minority of instances, preoxidation with Fe(VI) improved UV254 absorbance removal. In other instances, the impact was negligible compared to coagulation without any preoxidation. In continuous flow experiments, the addition of a Fe(VI) preoxidation step was found to improve UV254 absorbance, turbidity and DBP levels in finished water, as compared to treatment without preoxidation, without other negative water quality or operational impacts. However, for one source water, when $FeCl_3$ was added prior to polymer coagulation, the beneficial impact on water quality was essentially the same, indicating that interactions between Fe(III) and NOM, not oxidation of NOM by Fe(VI) were the controlling processes. Importantly, Fe(VI) is likely to provide additional benefits such as disinfection, and oxidation of specific inorganic and organic contaminants, impacts not achievable by Fe(III), and without some of the undesirable impacts of other strong oxidants. Operational concerns related to ferrate peroxidation were not noted for the continuous flow experiments.

APPENDIX

SUPPORTING INFORMATION

Table A.1 Water quality characteristics of Atkins Water

Parameter	Value	Units
Unadjusted pH	6.8	--
Unadjusted Alk.	72	μM as HCO_3^-
Turbidity	0.51	NTU
TOC	3.15	mg/L
DOC	3.01	mg/L
UV254 Abs.	0.085	cm^{-1}
SUVA	2.82	m^{-1}/mg/L DOC
Iron	0.05	mg/L
Manganese	0.02	mg/L

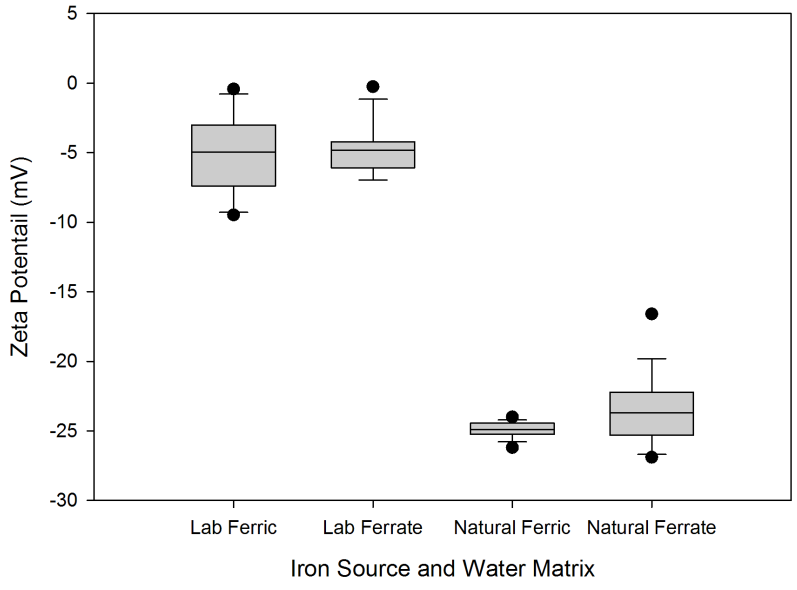

Figure A.1 Boxplot of zeta potential of ferrate and ferric resultant particles in lab and natural water matrices; 1 mM HCO_3^-, pH = 6.2, Fe = 3 mg/L

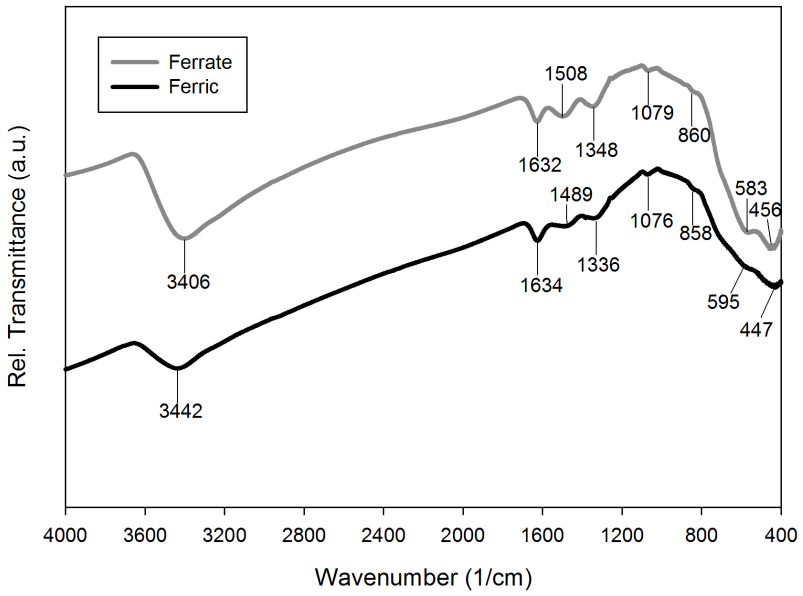

Figure A.2 Transmission FTIR spectra of ferric and ferrate resultant particles

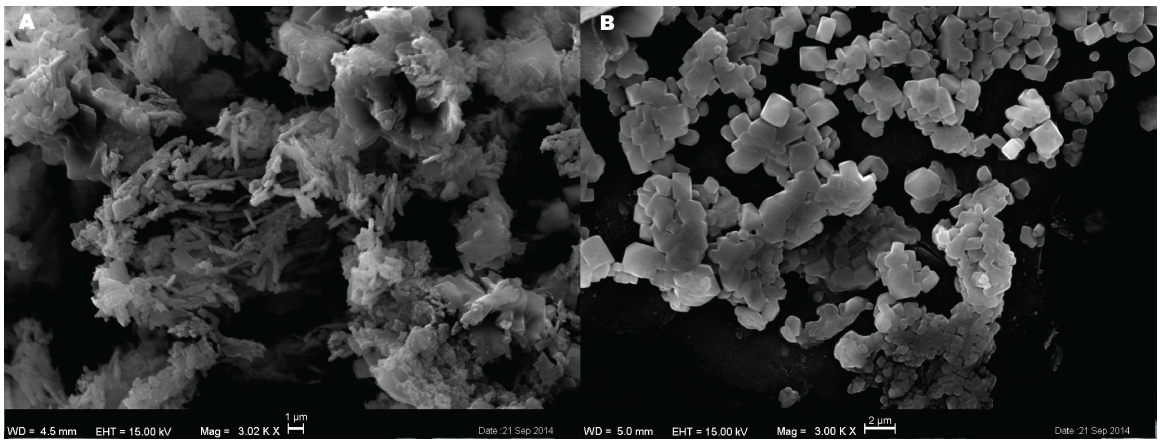

Figure A.3 Micrograph of particles from ferric (A) and ferrate (B) addition in natural water

Table A.2 Regression results from linear relationship between Fe(VI) dose and Mn(II) oxidized; DI water matrix: 1 mM HCO_3^-, $Mn(II)_i$ = 4.9 μM and 9.8 μM; NOM water matrix: 1 mM HCO_3^-, $Mn(II)_i$ = 4.9 μM and 9.8 μM, TOC = 1.75 mg/L; (yo = y-intercept, SE = standard error, a = slope)

Matrix	pH	y_o	y_o SE	a	a SE	R^2	N
DI	both	n/a	n/a	0.667	0.008	0.978	48
DI	6.2	n/a	n/a	0.667	0.009	0.982	36
DI	7.5	n/a	n/a	0.668	0.019	0.968	12
NOM	both	0.089	0.135	0.751	0.030	0.969	19
NOM	6.2	0.167	0.347	0.802	0.067	0.973	5
NOM	7.5	0.114	0.108	0.714	0.026	0.982	14

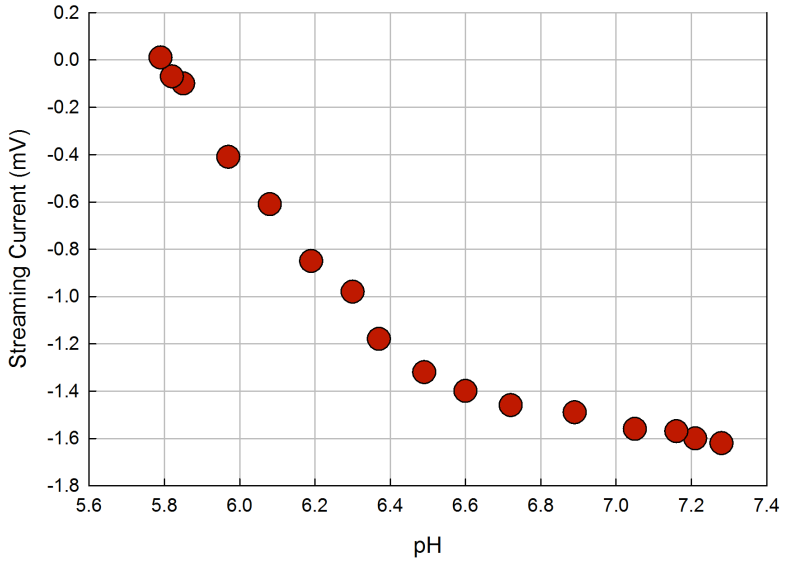

Figure A.4 Streaming current results from coagulant charge analyzer; 1 mM HCO_3^-, Mn(II) initial = 11 μM, Fe(VI) dose = 7.5 μM

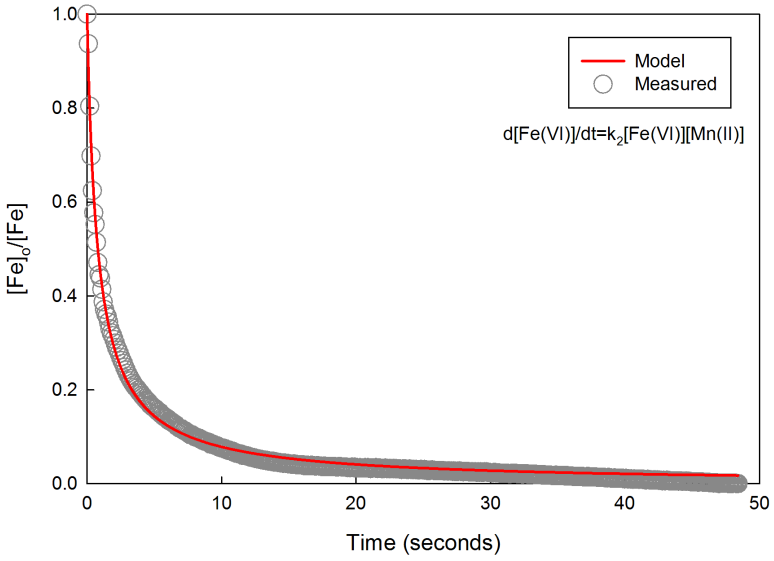

Figure A.5 Normalized Fe(VI) concentration decay measured via absorbance at 510nm with second order rate constant numerical approximation model; pH = 9.2; BO_3^{-3} = 0.2 mM, Fe(VI) initial = 75 μM, Mn(II) initial = 113 μM; estimated k_2 = 1.0×10^4 M^{-1} s^{-1}

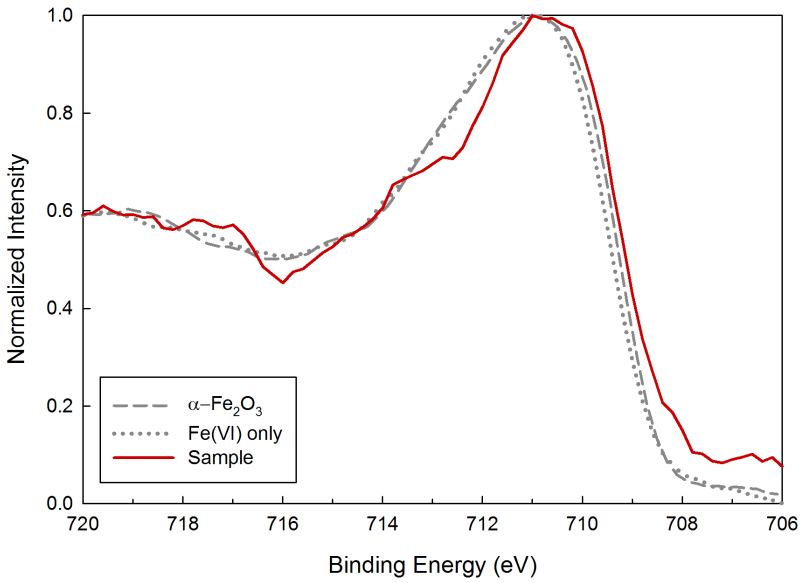

Figure A.6 Photoelectron spectra in the Fe $2p^{3/2}$ region of particles resulting from ferrate decay (e.g., Fe(VI) only), oxidation of Mn(II) by Fe(VI), and an Fe_2O_3 standard (hematite)

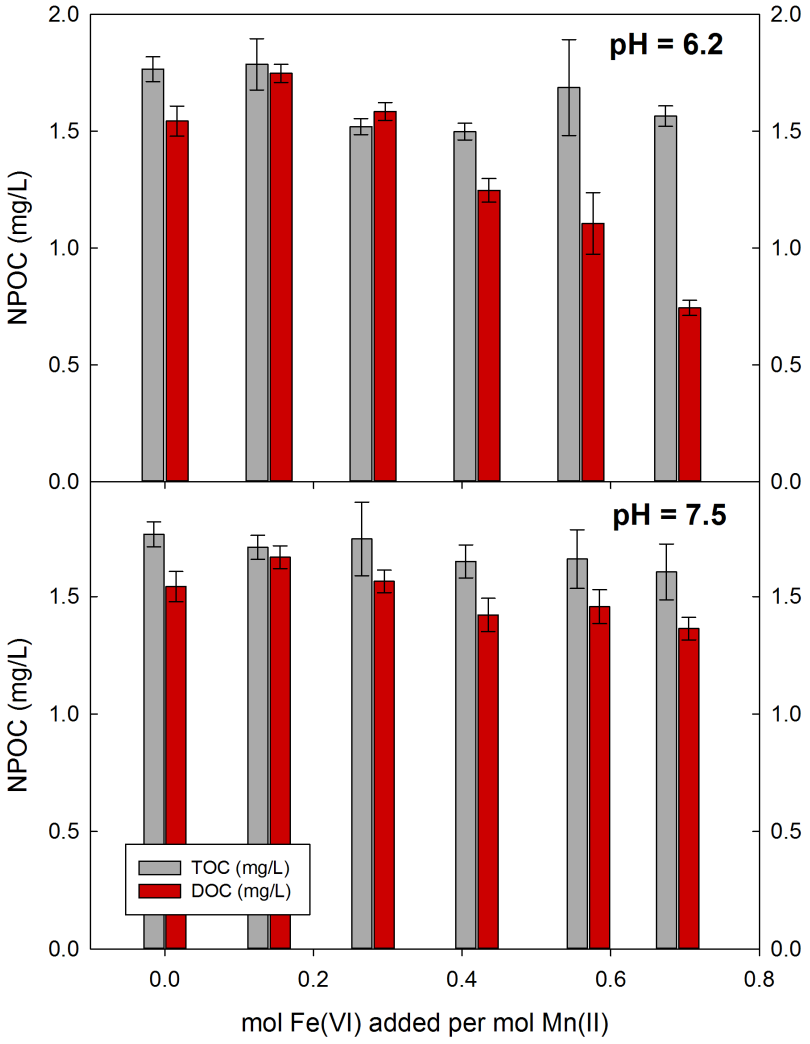

Figure A.7 TOC and DOC Mn(II) water matrix following various ferrate dosages; 1 mM HCO_3^-, (NPOC, nonpurgable organic carbon). Each bar represents the mean of 3 measurements, with error bars representing the positive and negative of one standard deviation

BIBLIOGRAPHY

Alsheyab, M., Jiang, J.-Q., Stanford, C., 2009. On-line production of ferrate with an electrochemical method and its potential application for wastewater treatment--a review. J. Environ. Manage. 90, 1350–6. doi:10.1016/j.jenvman.2008.10.001

APHA, AWWA, WEF, 2005. Standard Methods for the Examination of Water and Wastewater, 22nd ed, Standard Methods for the Examination of Water and Wastewater. Washington, DC.

Au, K.-K., Penisson, A.C., Yang, S., O'Melia, C.R., 1999. Natural organic matter at oxide/water interfaces: complexation and conformation. Geochim. Cosmochim. Acta 63, 2903–2917. doi:10.1016/S0016-7037(99)00268-9

AWWA, 2011. Water quality & treatment: a handbook on drinking water, Sixth. ed. McGraw-Hill, New York.

AWWA, ASCE, 1998. Water Treatment Plant Design, Third. ed. McGraw-Hill, New York.

Baalousha, M., 2009. Aggregation and disaggregation of iron oxide nanoparticles: Influence of particle concentration, pH and natural organic matter. Sci. Total Environ. 407, 2093–101. doi:10.1016/j.scitotenv.2008.11.022

Black, A., Singley, J., Whittle, G., Moulding, J., 1963. Stoichiometry of the coagulation of color-causing organic compounds with ferric sulfate. J. Am. Water Works Assoc. 55, 1347–1366.

Bose, P., Reckhow, D.A., 2007. The effect of ozonation on natural organic matter removal by alum coagulation. Water Res. 41, 1516–24. doi:10.1016/j.watres.2006.12.027

Bouchard, M.F., Sauvé, S., Barbeau, B., Legrand, M., Brodeur, M.-È., Bouffard, T., Limoges, E., Bellinger, D.C., Mergler, D., 2011. Intellectual impairment in school-age children exposed to manganese from drinking water. Environ. Health Perspect. 119, 138–43. doi:10.1289/ehp.1002321

Brandhuber, P., Clark, S., Knocke, W., Tobiason, J., 2013. Guidance for the Treatment of Manganese. Water Research Foundation, Denver, CO.

Burger, M.S., Mercer, S.S., Shupe, G.D., Gagnon, G.A., 2008. Manganese removal during bench-scale biofiltration. Water Res. 42, 4733–42. doi:10.1016/j.watres.2008.08.024

Carlson, K.H., Knocke, W.R., Gertig, K.R., 1997. Optimizing treatment through Fe and Mn fractionation. J. / Am. Water Work. Assoc. 89, 162–171.

Carr, J., 2008. Kinetics and product identification of oxidation by ferrate (VI) of water and aqueous nitrogen containing solutes, in: Sharma, V. (Ed.), ACS Symp. Ser. American Chemical Society, Washington, pp. 189–196.

Carr, J., Kelter, P., Tabatabai, A., Splichal, D., 1984. Properties of ferrate (VI) in aqueous solution: an alternate oxidant in wastewater treatment, in: Jolley, R., Bull, R., Davis, W., Katz, S., Roberts, M., Jabos, V. (Eds.), Water Chlorination: Chemistry, Environmental Impact and Health Effects. Lewis Publishers, Inc., Williamsburgh, pp. 1285–1298.

Cerrato, J.M., Hochella, M.F., Knocke, W.R., Dietrich, A.M., Cromer, T.F., 2010. Use of XPS to identify the oxidation state of Mn in solid surfaces of filtration media oxide samples from drinking water treatment plants. Environ. Sci. Technol. 44, 5881–5886. doi:10.1021/es100547q

Cerrato, J.M., Knocke, W.R., Hochella, M.F., Dietrich, A.M., Jones, A., Cromer, T.F., 2011. Application of XPS and solution chemistry analyses to investigate soluble manganese removal by MnOx(s)-coated media. Environ. Sci. Technol. 45, 10068–10074. doi:10.1021/es203262n

Chen, K.L., Elimelech, M., 2007. Influence of humic acid on the aggregation kinetics of fullerene (C60) nanoparticles in monovalent and divalent electrolyte solutions. J. Colloid Interface Sci. 309, 126–34. doi:10.1016/j.jcis.2007.01.074

Ciampi, L.E., Daly, L.J., 2009. Methods of synthesizing a ferrate oxidant and its use in ballast water. US7476342B2.

Coffey, B., Gallagher, D., Knocke, W., 1993. Modeling Soluble Manganees Removal By Oxide-Coated Filter Media. J. Environ. Eng. 119, 679–694.

Cornell, R.M., Giovanoli, R., Schneider, W., 1989. Review of the hydrolysis of iron(III) and the crystallization of amorphous iron(III) hydroxide hydrate. J. Chem. Technol. Biotechnol. 46, 115–134.

DeLuca, S., Chao, A., Smallwood, C., 1983. Ames test of ferrate treated water. J. Environ. Eng. 109, 1159–1167.

Duan, J., Gregory, J., 2003. Coagulation by hydrolysing metal salts. Adv. Colloid Interface Sci. 100-102, 475–502. doi:10.1016/S0001-8686(02)00067-2

Dumais, O., 1990. Pilot Plant Evaluation for Atkins Reservoir. Westfield, MA.

Edwards, M., Benjamin, M., 1992. Transformation of NOM by Ozone and its Effect on Iron and Aluminum Solubility. J. Am. Water Works Assoc. 84, 56–66.

Edwards, M., Benjamin, M., Tobiason, J., 1994. Effects of ozonation on coagulation of NOM using polymer alone and polymer/metal salt mixtures. J. Am. Water Works Assoc. 86, 105–116.

Edzwald, J., 1993. Coagulation in drinking water treatment: Particles, organics and coagulants. Water Sci. Technol. 27, 21–35.

Edzwald, J.K., Becker, W.C., Wattier, K.L., 1985. Surrogate parameters for monitoring organic matter and THM precursors. J. / Am. Water Work. Assoc. 77, 122–131.

Edzwald, J.K., Tobiason, J.E., 1999. Enhanced coagulation: US requirements and a broader view. Water Sci. Technol. 40, 63–70. doi:10.1016/S0273-1223(99)00641-1

Flynn Jr., C.M., 1984. Hydrolysis of inorganic iron(III) salts. Chem. Rev. 84, 31–41. doi:10.1021/cr00059a003

Gan, W., Sharma, V.K., Zhang, X., Yang, L., Yang, X., 2015. Investigation of Disinfection Byproducts Formation in Ferrate(VI) Pre-Oxidation of NOM and its Model Compounds followed by Chlorination. J. Hazard. Mater. doi:10.1016/j.jhazmat.2015.02.037

Gilbert, M.B., Waite, T.D., Hare, C., 1976. Analytical Notes - An Investigation of the Applicability of Ferrate Ion for Disinfection. J. / Am. Water Work. Assoc. 68, 495–497.

Gombos, E., Felföldi, T., Barkács, K., Vértes, C., Vajna, B., Záray, G., 2012. Ferrate treatment for inactivation of bacterial community in municipal secondary effluent. Bioresour. Technol. 107, 116–21. doi:10.1016/j.biortech.2011.12.053

Goodwill, J., Jiang, Y., Tobiason, J., Reckhow, D., 2014. Pilot-scale assessment of ferrate Pre-oxidation, in: Proceedings of the AWWA Annual Conference and Exposition (ACE14). American Water Works Association, Denver, CO.

Goodwill, J.E., Jiang, Y., Reckhow, D.A., Gikonyo, J., Tobiason, J.E., 2015. Characterization of Particles from Ferrate Preoxidation. Environ. Sci. Technol. 49, 4955–4962. doi:10.1021/acs.est.5b00225

Gordon, G., Slootmaekers, B., Tachiyashiki, S., Wood, D., 1990. Minimizing chlorite ion and chlorate ion in water treated with chlorine dioxide. J. Am. Water Works Assoc. 82, 160–165.

Gotić, M., Musić, S., 2007. Mössbauer, FT-IR and FE SEM investigation of iron oxides precipitated from FeSO4 solutions. J. Mol. Struct. 834-836, 445–453. doi:10.1016/j.molstruc.2006.10.059

Graham, N., Khoi, T., Jiang, J., 2010. Oxidation and Coagulation of Humic Substances by Potassium Ferrate. Water Sci. Technol. 62, 929–936.

Gregory, D., Carlson, K., 2003. Effect of soluble Mn concentration on oxidation kinetics. J. Am. Water Works Assoc. 95, 98–108.

Gu, B., Schmitt, J., Chen, Z., 1994. Adsorption and desorption of natural organic matter on iron oxide: mechanisms and models. Environ. Sci. Technol. 28, 38–46.

He, Q., Leppard, G., Paige, C., Snodgrass, W., 1996. Transmission Electron Microscopy of a Phosphate Effect on the Colloid Structure if Iron Hydroxide. Water Res. 30, 1345–1352.

Hu, L., Page, M., Marinas, B., Shisler, J., Strathmann, T., 2008. Treatment of emerging pathogens and micropollutants with potassium ferrate (VI), in: American Water Works Association 2008 WQTC Proceedings. American Water Works Association, Cincinnati, pp. 1–8.

Huang, H., Sommerfeld, D., Dunn, B.C., Eyring, E.M., Lloyd, C.R., 2001. Ferrate(VI) Oxidation of Aqueous Phenol: Kinetics and Mechanism. J. Phys. Chem. 105, 3536–3541. doi:10.1021/jp0039621

Hudson, H.E., Wagner, E.G., 1981. Conduct and uses of jar tests. J. / Am. Water Work. Assoc. 73, 218–223.

Islam, A., Goodwill, J., Bouchard, R., Tobiason, J., Knocke, W., 2010. Characterization of filter and media MnOx (s) surfaces and Mn removal capability. J. Am. Water Work. Assoc. 102, 71–83.

Jiang, J., Pang, S.-Y., Ma, J., Liu, H., 2012. Oxidation of phenolic endocrine disrupting chemicals by potassium permanganate in synthetic and real waters. Environ. Sci. Technol. 46, 1774–81. doi:10.1021/es2035587

Jiang, J., Wang, S., 2003. Enhanced coagulation with potassium ferrate (VI) for removing humic substances. Environ. Eng. Sci. 20, 2003.

Jiang, J.-Q., Lloyd, B., 2002. Progress in the development and use of ferrate(VI) salt as an oxidant and coagulant for water and wastewater treatment. Water Res. 36, 1397–408.

Jiang, J.-Q., Wang, S., Panagoulopoulos, A., 2006. The exploration of potassium ferrate(VI) as a disinfectant/coagulant in water and wastewater treatment. Chemosphere 63, 212–9. doi:10.1016/j.chemosphere.2005.08.020

Jiang, W., Chen, L., Batchu, S.R., Gardinali, P.R., Jasa, L., Marsalek, B., Zboril, R., Dionysiou, D.D., O'Shea, K.E., Sharma, V.K., 2014. Oxidation of Microcystin-LR by Ferrate(VI): Kinetics, Degradation Pathways, and Toxicity Assessments. Environ. Sci. Technol. doi:10.1021/es5030355

Jiang, Y., Goodwill, J.E., Reckhow, D.A., Tobiason, J.E., 2014. Ferrate decomposition in natural waters and impacts on natural organic matter and disinfection by-product precursors, in: Proceedings of the AWWA Annual Conference and Exposition (ACE14). American Water Works Association, Denver, CO.

Jiang, Y., Goodwill, J.E., Tobiason, J.E., Reckhow, D.A., 2015. Effect of Different Solutes, Natural Organic Matter, and Particulate Fe(III) on Ferrate(VI) Decomposition in Aqueous Solutions. Environ. Sci. Technol. 49, 2841–2848. doi:10.1021/es505516w

Knocke, W., Ramon, J., Thompson, C., 1988. Soluble manganese removal on oxide-coated filter media. J. Am. Water Works Assoc. 80, 65–70.

Knocke, W., Van Benschoten, J., Kearney, M., Soborski, A., Reckhow, D.A., 1991. Kinetics of Manganese and Iron Oxidation by Potassium Permanganate and Chlorine Dioxide. J. Am. Water Work. Assoc. 83, 80–87.

Knocke, W.R., Zuravnsky, L., Little, J.C., Tobiason, J.E., 2010. Adsorptive contactors for removal of soluble manganese during drinking water treatment. J. / Am. Water Work. Assoc. 102, 64–75.

Kohl, P.M., Medlar, S.J., 2006. Occurrence of manganese in drinking water and manganese control. American Water Works Association, Denver, CO.

Lee, Y., Kissner, R., von Gunten, U., 2014. Reaction of ferrate(VI) with ABTS and self-decay of ferrate(VI): kinetics and mechanisms. Environ. Sci. Technol. 48, 5154–62. doi:10.1021/es500804g

Lee, Y., Um, I., Yoon, J., 2003. Arsenic(III) oxidation by iron(VI) (ferrate) and subsequent removal of arsenic(V) by iron(III) coagulation. Environ. Sci. Technol. 37, 5750–6.

Lee, Y., Yoon, J., von Gunten, U., 2005a. Spectrophotometric determination of ferrate (Fe(VI)) in water by ABTS. Water Res. 39, 1946–1953.

Lee, Y., Yoon, J., von Gunten, U., 2005b. Kinetics of the oxidation of phenols and phenolic endocrine disruptors during water treatment with ferrate (Fe(VI)). Environ. Sci. Technol. 39, 8978–8984.

Lee, Y., Zimmermann, S.G., Kieu, A.T., Von Gunten, U., 2009. Ferrate (Fe(VI)) application for municipal wastewater treatment: A novel process for simultaneous micropollutant oxidation and phosphate removal. Environ. Sci. Technol. 43, 3831–3838. doi:10.1021/es803588k

Lim, M., Kim, M.-J., 2009. Removal of Natural Organic Matter from River Water Using Potassium Ferrate(VI). Water. Air. Soil Pollut. 200, 181–189. doi:10.1007/s11270-008-9902-x

Lytle, D., Snoeyink, V., 2002. Effect of ortho-and polyphosphates on the properties of iron particles and suspensions. Journal-American Water Work. Assoc. 94, 87.

Ma, J., Liu, W., 2002a. Effectiveness of ferrate (VI) preoxidation in enhancing the coagulation of surface waters. Water Res. 36, 4959–4962.

Ma, J., Liu, W., 2002b. Effectiveness and mechanism of potassium ferrate(VI) preoxidation for algae removal by coagulation. Water Res. 36, 871–878. doi:10.1016/S0043-1354(01)00282-2

Merkle, P.B., Knocke, W.R., Gallagher, D.L., 1997. Method for Coating Filter Media with Synthetic Manganese Oxide. J. Environ. Eng. 123, 642–649. doi:10.1061/(ASCE)0733-9372(1997)123:7(642)

Monzyk, B.F., Rose, J.K., Burckle, E.C., Smeltz, A.D., Rider, D.G., Cucksey, C.M., Clark, T.O., 2013. Method for producing ferrate (V) and/or (VI). US8449756B2.

Mouchet, P., 1992. From conventional to biological removal of iron and manganese in France. J. / Am. Water Work. Assoc. 84, 158–167.

Moulder, J.F., Chastain, J., King, R.C., 1992. Handbook of X-ray photoelectron spectroscopy: a reference book of standard spectra for identification and interpretation of XPS data. Perkin-Elmer, Eden Prairie.

Music, S., Nomura, K., Popovic, S., 1998. Microstructural properties of Fe – oxide powders obtained by precipitation from FeCl 3 solutions. Mater. Sci. Eng. B 56, 43–52.

Netzer, A., Bowers, A., Norman, J.D., 1973. Removal of Trace Metals from Wastewater by Lime and Ozonation, in: Barrekette, E. (Ed.), Pollution, Environmental Science Research. Springer US, pp. 380–386. doi:10.1007/978-1-4899-0330-3_33

Norgren, K., Winklemeyer, B., Conley, W., 1993. Pilot Study Report: Trident Water Systems. Strubridge, MA.

O'Melia, C., Becker, W., Au, K., 1999. Removal of humic substances by coagulation. Water Sci. Technol. 40, 47–54. doi:10.1016/S0273-1223(99)00639-3

Ockerman, L., Schreyer, J., 1951. Preparation of Sodium Ferrate(VI) 72, 5478.

Prucek, R., Tuček, J., Kolařík, J., Filip, J., Marušák, Z., Sharma, V.K., Zbořil, R., 2013. Ferrate(VI)-induced arsenite and arsenate removal by in situ structural incorporation into magnetic iron(III) oxide nanoparticles. Environ. Sci. Technol. 47, 3283–92. doi:10.1021/es3042719

Reckhow, D.A., Knocke, W.R., Kearney, M.J., Parks, C.A., 1991. Oxidation Of Iron And Manganese By Ozone. Ozone Sci. Eng. 13, 675–695. doi:10.1080/01919512.1991.10555708

Schwertmann, U., Cornell, R.M., 2008. Iron oxides in the laboratory. John Wiley & Sons.

Sharma, V., 2002. Potassium ferrate (VI): an environmentally friendly oxidant. Adv. Environ. Res. 2002, 143–156.

Sharma, V., 2007. Disinfection performance of Fe (VI) in water and wastewater: a review. Water Sci. Technol. 55, 225–232.

Sharma, V., Jiang, J., Kim, H., 2013. Ferrate(VI): Novel Compound for Removal of Natural Organic Matter in Water, in: Xu, J., Wu, J., He, Y. (Eds.), Functions of Natural Organic Matter in Changing Environment SE - 166. Springer Netherlands, pp. 911–914. doi:10.1007/978-94-007-5634-2_166

Sharma, V.K., 2002. Ferrate(V) oxidation of pollutants: a premix pulse radiolysis study. Radiat. Phys. Chem. 65, 349–355. doi:10.1016/S0969-806X(02)00335-3

Sharma, V.K., 2010. Oxidation of inorganic compounds by Ferrate(VI) and Ferrate(V): one-electron and two-electron transfer steps. Environ. Sci. Technol. 44, 5148–52. doi:10.1021/es1005187

Sharma, V.K., 2011. Oxidation of inorganic contaminants by ferrates (VI, V, and IV)--kinetics and mechanisms: a review. J. Environ. Manage. 92, 1051–73. doi:10.1016/j.jenvman.2010.11.026

Sharma, V.K., Kazama, F., Jiangyong, H., Ray, A.K., 2005. Ferrates (iron(VI) and iron(V)): environmentally friendly oxidants and disinfectants. J. Water Health 3, 45–58.

Sharma, V.K., Mishra, S.K., 2006. Ferrate(VI) oxidation of ibuprofen: A kinetic study. Environ. Chem. Lett. 3, 182–185. doi:10.1007/s10311-005-0002-5

Sharp, E.L., Jarvis, P., Parsons, S. a, Jefferson, B., 2006. The impact of zeta potential on the physical properties of ferric--NOM flocs. Environ. Sci. Technol. 40, 3934–40.

Sinsabaugh, R.L., Hoehn, R.C., Knocke, W.R., Linkins, A.E., 1986. Removal of dissolved organic carbon by coagulation with iron sulfate. J. / Am. Water Work. Assoc.

Soucie, B., Madura, R., Sandahl, M., Nitecki, K., 2003. Wilson Wins Top Prize in 2003 Contest. Opflow 12.

Stumm, W., 1992. Chemistry of the solid-water interface: processes at the mineral-water and particle-water interface in natural systems. New York, NY (United States); John Wiley Sons, New York.

Stumm, W., Morgan, J., Black, A., 1962. Chemical aspects of coagulation. J. Am. Water Works Assoc. 54, 971–994.

Stumm, W., O'Melia, C., 1968. Stoichiometry of Coagulation. J. Am. Water Works Assoc. 60, 514–539.

Thompson, G., Ockerman, L., Schreyer, J., 1951. Preparation and purification of Potassium Ferrate VI. J. Am. Chem. Soc. 73, 1379–1381. doi:10.1021/ja01147a536

Tipping, E., 1981. The adsorption of aquatic humic substances by iron oxides. Geochim. Cosmochim. Acta 45, 191–199. doi:10.1016/0016-7037(81)90162-9

Tipping, E., Heaton, M.J., 1983. The adsorption of aquatic humic substances by two oxides of manganese. Geochim. Cosmochim. Acta 47, 1393–1397. doi:10.1016/0016-7037(83)90297-1

Tobiason, J.E., Knocke, W.R., Goodwill, J., Hargette, P., Bouchard, R., Zuravnsky, L., 2008. Characterization and Performance of Filter Media for Manganese Control. Water Research Foundation, Denver, CO.

Vermeer, A., Riemsdijk, W. Van, Koopal, L., 1998. Adsorption of Humic Acid to Mineral Particles 1. Specific and Electrostatic Interactions. Langmuir 14, 2810–2819.

Von Gunten, U., 2003. Ozonation of drinking water: part II. Disinfection and by-product formation in presence of bromide, iodide or chlorine. Water Res. 37, 1469–87. doi:10.1016/S0043-1354(02)00458-X

Werdehoff, K., Singer, P., 1987. Chlorine dioxide effects on THMFP, TOXFP, and the formation of inorganic by-products. J. Am. Water Works Assoc. 79, 107–113.

Wood, R., 1958. The Heat, Free Energy and Entropy of the Ferrate(VI) Ion. J. Am. Chem. Soc. 80, 2038–2041. doi:10.1021/ja01542a002

Yang, B., Ying, G.-G., Zhao, J.-L., Zhang, L.-J., Fang, Y.-X., Nghiem, L.D., 2011. Oxidation of triclosan by ferrate: reaction kinetics, products identification and toxicity evaluation. J. Hazard. Mater. 186, 227–35. doi:10.1016/j.jhazmat.2010.10.106

Yates, B.J., Zboril, R., Sharma, V.K., 2014. Engineering aspects of ferrate in water and wastewater treatment – a review. J. Environ. Sci. Heal. Part A 49, 1603–1614. doi:10.1080/10934529.2014.950924